Gelation By Design

Green, Bradley

2026

Document Version:
Publisher's PDF, also known as Version of record

Gelation By Design

BRADLEY GEORGE GREEN | CENTRE FOR ANALYSIS AND SYNTHESIS | LUND UNIVERSITY

Printed by Media-Tryck, Lund 2026 NORDIC SWAN ECOLABEL 3041 0903

LUND UNIVERSITY

ISBN 978-91-90202-87-6

Centre for Analysis and Synthesis
Department of Chemistry
Faculty of Engineering
Lund University

9 789190 202876

Gelation By Design

Gelation By Design

by Bradley George Green

LUND
UNIVERSITY

Thesis for the degree of Doctor of Philosophy
Thesis advisors: Prof. Karen Edler
Faculty opponent: Prof. João Cabral

To be presented, with the permission of the Faculty of Engineering of Lund University, for public criticism in Lecture Hall A (KC:A) at the Centre for Analysis and Synthesis on Monday, the 14th of September 2026 at 09:00.

Organization
LUND UNIVERSITY

Centre for Analysis and Synthesis
Lund University
SE–223 62 LUND
Sweden

Document name
DOCTORAL DISSERTATION

Date of disputation
2026-09-14

Sponsoring organization
UNILEVER R&D

Port Sunlight, Quarry Road East, Bebington, Birkenhead, Wirral CH63 3JW, UK

Author(s)
Bradley George Green

Title and subtitle
Gelation By Design

Abstract
In order to meet the demands of consumers, personal care products, like any other product, must undergo constant innovation in order to stay up to date with consumer needs, preferences whilst conforming to commercial regulation. Here, the works contained within this thesis firstly aim to gain greater understanding of current actives in aluminium antiperspirant products, through the manufacture and use of a custom built *in situ* SAXS microfluidic device, which is discussed in Paper I. This study aimed to observe the gel formation and therefore eccrine sweat gland plugging capabilities of aluminium antiperspirants within a model environment.

Secondly, we studied type V eutectic solvent mixtures as potential novel carriers for personal care products, but with a focus on the fundamental interactions occurring within the systems rather than an application based approach. These solvents are novel, composing of mixtures of non-ionic hydrogen bond donors and hydrogen bond acceptors. Their simple preparation, without the need for elaborate synthesis or expensive chemicals, makes them accessible to chemists both in the research lab and potentially industrially. They are normally are composed of naturally sourced, environmentally benign compounds such as fatty acids and terpenes, which causes them to be hydrophobic and considered much more 'green' compared to petrochemically derived oils, which they are suggested as suitable candidates to replace. A (deep) eutectic solvent was used initially as the dispersed (droplet) phase in an emulsion system in Paper II. In this study, the addition of stearate salts to the droplet phase formulations were found to affect the surfactant packing of non-ionic poloxamer surfactants at the emulsion interface, improving the emulsion stability.

Finally, in Paper III, the tunable nature of 25 ES mixtures were explored by comparing the gelation properties of the low molecular weight gelator, 12-hydroxystearic acid, within them. This work compared how the pairings of compounds in the ES mixtures interacted via hydrogen bonding with themselves and in turn the HSA, to form a range of eutectogels, illustrating the tunable nature of these novel solvents.

Key words
(Deep) Eutectic Solvents, Gelation, Nanoscience, SANS, SAXS, Scattering, Self-Assembly, Soft Matter, Surfactants, Rheology,

Classification system and/or index terms (if any)

Supplementary bibliographical information

Language
English

ISSN and key title

ISBN
978-91-90202-87-6 (print)
978-91-90202-88-3 (pdf)

Recipient's notes

Number of pages
165

Price

Security classification

Signature _____ Date 2026-06-18

Gelation By Design

by Bradley George Green

LUND
UNIVERSITY

A doctoral thesis at a university in Sweden takes either the form of a single, cohesive research study (monograph) or a summary of research papers (compilation thesis), which the doctoral student has written alone or together with one or several other author(s).

In the latter case the thesis consists of two parts. An introductory text puts the research work into context and summarizes the main points of the papers. Then, the research publications themselves are reproduced, together with a description of the individual contributions of the authors. The research papers may either have been already published or are manuscripts at various stages (in press, submitted, or in draft).

Cover illustration front: Twisted HSA fibres, formed within a chiral DES, which features in Paper III

Cover illustration back: Picture showing me and friends, sailing in the Öresund.

Funding information: The thesis work was financially supported by Unilever R&D, Port Sunlight, UK.

Faculty of Engineering, Centre for Analysis and Synthesis

ISBN: 978-91-90202-87-6 (print)
ISBN: 978-91-90202-88-3 (pdf)
ISSN:

Printed in Sweden by Media-Tryck, Lund University, Lund 2026

Solvitur Ambulando

— Diogenes the Cynic

Contents

Acknowledgements

A PhD thesis is not written in isolation, and I am very grateful to those who have supported me along the way. Firstly, I would like to thank my supervisors; Karen, Emily, Viveka and Andreas for the opportunity to pursue this venture and for their guidance throughout. I also thank Unilever R%D for providing financial support, without which my PhD studies wouldn't have been possible.

To Sara, Maria, Åse and Kornelije, thank you for all your work in CAS. You are an integral part to ensuring everything runs smoothly and there is so much you do which goes unseen. Sara, in particular, you went over and above your role in CAS, helping me to feel like part of the department and at home in Sweden. You have always been there for us to put the world to rights over a coffee or a beer. I hope we will stay in close contact in the future.

To Alice, you have been a rock from the start, from when I applied for PhD positions after the pandemic to the very end of my doctoral studies. I would not have started this journey without your support and certainly could not have finished it.

Whilst the unexpected move from Bath to Lund was a shock to the system, it brought so many opportunities. It allowed me allowed to meet many good people, from all walks of life. To my fellow PhD students and post-docs in the Edler group; I wish you all the best. You have all provided me with many memories during this time, travelling to beamtimes with you has been fun, despite the long nights and experiments we wished turned out slightly differently. I hope I made the group a bit more of a better place to work. To Ronak, Nguyen and Maggie, you still have a bit of time to go but I'm sure it will all work out great.

To Petteri, your ability to sift the wheat from the chaff, paired with your superb work ethic, is an inspiration to me and many others. You are also a good friend and have helped me make the best of every situation.

I also had the pleasure of sharing the office with a few great visitors to the lab. However, two stand out; Matheus, you helped me so much when you visited the group and became a friend I never expected to make. Your friendly, hard-working attitude made it a pleasure to work with you, where you encouraged me where I could see nowhere to move forward. Visiting you in Rio was really cool and I hope to have a proper catch up soon! Gianluca, your wicked sense of humour and perfect timing is killer, it will be great to catch up in Granada and all the best for the rest of the PhD!

To my CAS colleagues, those pub trips into town on Friday evenings were a well needed tonic to add a little stretch to the strain of everyday life. I especially would like to thank my material chemistry colleagues; Azemina, Aidas, Hedda and Edvin, you made the world seem that little bit warmer and brighter. A big thanks to Reine, who made me feel welcome from the first day and throughout my time in the department.

To Fredrik, Joachim, Nils and Roberto; you guys have been a laugh the whole time, it's been great. Róisín, you always brightened my mood and I'm glad we agree that Yorkshire Tea is superior.

I am also very thankful to everyone who encouraged me to learn Swedish. Your patience and openness, whether it be through teaching me new words and phrases or including me in your culture and traditions means so much to me. I shall carry these with me wherever I go.

To Rebecka and Victor, the riding, jumping (and the occasional spontaneous dismount!) with Orion and Vargen were a wonderful distraction, thank you so much.

Last, but by no means least, to Fanny: you have made the last part of my PhD very special. I hope I can support you in your PhD as you have supported me during mine. I am always amazed at how you can see the world from an alternative view, which has allowed me to relax from so many problems and enjoy our time together.

Popular Science Summary

Ever since the antiperspirant property of aluminium chloride was discovered in the 1950s, aluminium based antiperspirant products have exploded in popularity across the globe. Today, antiperspirant products are available in a myriad of applicators including aerosols, creams, lotions, sticks and emulsions. In order to cater to consumer needs, these products are continuously evolving. This ensures that the products are as efficacious, user friendly, compliant to regulation, cost effective and as environmentally friendly as possible.

This work explores several aspects of antiperspirant technology. Firstly, with a study which sought to further explore the mechanism of antiperspirant salt function. This used a custom made microfluidic device, which simulated the sweat glands naturally occurring in our skin. This device was designed for optimal performance in synchrotron small angle X-ray scattering (SAXS) experiments, which allowed high quality data to be collected in short exposure times, allowing fast data collection and therefore a mapping an area within the microfluidic channel in the shortest time possible. This work is discussed in Paper I.

After this, the project focus shifted towards potential novel carriers for personal care products, where deep eutectic solvents (DES) have shown promise. Currently, these carriers are oils derived from mineral oils from petrochemical sources, they function well, but replacing them could be an opportunity to make them more environmentally and user friendly. For this, DES are a novel class of solvents which feature a great deal of potential. This is chiefly due to their favourable biodegradability and tunability which allows them to be suited to a broad range of applications. DES comprise pure mixtures of two or more chemical compounds which, whilst most of the compounds used are solid at room temperature, when they are combined at the correct ratio, they form a liquid due to a 'eutectic' depression of their melting points. This is due to interactions between the compounds, which makes them more energetically favourable to be combined in a mixture than apart. This effect is used every year on wintry roads, where rock salt is added to the surface to lower the melting point of ice, allowing it to be water at sub-zero temperatures.

These DES are categorised by the components of which they comprise. There are five of these 'types' and the components range from metal salts to alcohols and acids. However, for the works within this thesis, type V DES were employed, which consist of non-ionic hydrogen bond donors and acceptor molecules. These DES are considered 'green' as they consist of biodegradable compounds. These compounds are typically essential oils and fatty acids and are naturally

occurring, many of which can be derived from plants such as mint (menthol) and coconut oil (dodecanoic acid) in high purities. A benefit of essential oils as the components for DES, is that the solvents can feature the skin-safe and therapeutic properties of the components of which they comprise, bolstering the benefits of their use in personal care and pharmaceutical applications.

The pairing of components which form these liquid solvents at room temperature feature complex but amorphous networks of hydrogen bonds within the liquid phase, which allows many of the intriguing properties of the solvent to be manifested. These DES have low vapour pressures, meaning that they can function safely at elevated temperatures, without excessive evaporation. As they are hydrophobic with relatively low viscosity, they can function as potential replacements to petrochemical derived oils or solvents.

These novel solvents are both very interesting from a applied and fundamental perspective. Within this thesis both of these aspects are involved; In Paper II these solvents are used as the droplet phase in an emulsion system where the DES is used in the place of a petrochemical oil. In Paper III, gels are explored in an array of Type V ES, where the nature of the ES itself is seen to affect gel formation of a commonly studied gelator molecule. Here it was noted that the stoichiometry and even the chirality (handedness) of the DES components affected the nature of the gel network formed within.

List of Papers

This thesis is based on the following publications, referred to by their Roman numerals:

I **A Microfluidic Study of the Eccrine Sweat Gland Environment with a High Transmission SAXS Device**
B.G. Green, P. Mota-Santiago, E.R. Cross and K.J. Edler
manuscript

II **Emulsions of Hydrophobic Deep Eutectic Solvents Stabilised with Poloxamer Surfactants and Stearate Salts**
B.G. Green, M.O. Ferreira, P.A. Vainikka, K. Ma, D.A. Venero, A. Terry, E.R. Cross and K.J. Edler
Journal of Colloid and Interface Science, **2026**, 723, 140901

III **Gelation of 12-Hydroxystearic Acid in Type V Eutectic Solvents**
B.G. Green, A.J. Smith, E.R. Cross and K.J. Edler
manuscript

Author contributions

Paper I: A Microfluidic Study of the Eccrine Sweat Gland Environment with a High Transmission SAXS Device I planned and conducted the experiments, designed and fabricated the microfluidic devices, analysed the findings and wrote the first draft of the manuscript and edited the manuscript with co-authors input.

Paper II: Emulsions of Hydrophobic Deep Eutectic Solvents Stabilised with Poloxamer Surfactants and Stearate Salts

I conceptualised the idea for the experiments, formulated samples, conducted experiments, analysed the findings, wrote the original draft of the manuscript, edited the manuscript with co-authors input and prepared the manuscript for submission.

Paper III: Gelation of 12-Hydroxystearic Acid in Type V Eutectic Solvents

I conceptualised the idea for the experiments, formulated the samples, conducted the experiments, analysed the findings, wrote the first draft of the manuscript.

Abbreviations

AP - Antiperspirant
(A)ACH - (Activated) Aluminium Chlorohydrate
ASCH - Aluminium Sesquichlorohydrate
AZAG - Aluminium Zirconium Chlorohydrex and Glycine
BSA - Bovine Serum Albumen
CaSt - Calcium Stearate
CMC - Critical Micelle Concentration **COC** - Cyclic Olefin Copolymer
CPP - Critical Packing Parameter
(D)ES - (Deep) Eutectic Solvent
DSC - Differential Scanning Calorimetry
HBA - Hydrogen Bond Acceptor
HBD - Hydrogen Bond Donor
HLB - Hydrophilic Liphophilic Balance
HSA - 12-Hydroxy Stearic Acid
IEP - Isoelectric Point
IL - Ionic Liquid
LMWG - Low Molecular Weight Gelator
MgSt - Magnesium Stearate
MS - Mastersizer
NaSt - Sodium Stearate
P182 - Poloxamer 182
P184 - Poloxamer 184
P334 - Poloxamer P334
P407 - Poloxamer P407
PEEK - Poly Ethyl Ether Ketone
PEO - Polyethylene Oxide
PPO - Polypropylene Oxide
POM - Polarised Optical Microscopy
SANS - Small Angle Neutron Scattering
SAS - Small Angle Scattering
SAXS - Small Angle X-ray Scattering
TGA - Thermogravimetric Analysis
UP - Ultra Pure

ρ - Scattering Length Density
ρ_m - Mass Density

Constants

Planck's constant (h) = 6.626×10^{-34} J.s
Boltzmann's constant (K_B) = 1.381×10^{-23} J.K^{-1}
mass of an electron (m_e) = 9.109×10^{31} kg
mass of a neutron (m_n) = 1.675×10^{27} kg
speed of light in a vacuum (c) = 2.998×10^{8} m.s^{-1}
charge on an electron (e) = 1.602×10^{-19} C
classical electron radius(r_e) = 2.81×10^{-15} m

Gelation By Design: Research Context

The important thing in science is not so much to obtain new facts as to discover new ways of thinking about them.

— William Lawrence Bragg

Objectives of the Thesis

This thesis has two main objectives, which are summarised across three manuscripts submitted to the thesis. These three projects are connected by the research topic of antiperspirants and by the application of the small angle X-ray scattering technique which was used across all three projects.

1 Extend The Understanding of Current Antiperspirant Actives

The first aim was to achieve understanding of the current antiperspirant actives used in personal care products today, broadening the knowledge of the function of these aluminium salts as discussed in Chapters 2 and 3. The findings regarding this part of the thesis is summarised in Paper I.

2 Contribute to The Developments in Antiperspirant Technology

This second aim was rather flexible. This allowed me to develop interest in the potential of using alternative carriers for antiperspirant formulations. Therefore, the environmental benefits of using deep eutectic solvents as replacements for commonly used solvents seemed a rather appealing. Therefore, I formulated emulsions using a dodecanoic acid and menthol based DES, discussed in Paper II. After the first foray into the use of hydrophobic DES, I explored eutectogels with tunable properties, as discussed in Paper III. These studies illustrate the potential for DES to be used in personal care products as alternative carriers to the petrochemical based oils currently used.

Introduction

Antiperspirants are used everyday across the entire globe, to suit a variety of consumer needs and preferences, whilst conforming to ever evolving regulation. Therefore, constant innovation is required to consistently provide high quality personal care products, this thesis aims to contribute to the knowledge within this field. The following chapters introduce the fundamental techniques necessary to put the Papers I-III into context within the thesis.

Thesis Outline

All three of the papers within this thesis are heavily reliant on the use of small angle scattering of X-rays and neutrons as a versatile analysis technique. The fundamentals of this topic are laid out in Chapter 1.

Paper I: A Microfluidic Study of the Eccrine Sweat Gland Environment with a High Transmission SAXS Device

This paper explores and attempts to extend the current state of the art as far as the modelling of the eccrine sweat gland environment is concerned. The two parts of this project can be broken down into the chemistry of aluminium salts, which are explained in Chapter 2, and the application of this chemistry into the microfluidic environment, which is explained in Chapter 3.

Paper II: Emulsions of Hydrophobic Deep Eutectic Solvents Stabilised with Poloxamer Surfactants and Stearate Salts

From this point in the thesis, the work moves focus to the second thesis objective mentioned in the previous chapter; the development of novel carrier solutions for antiperspirant products. This work relies on the use of hydrophobic Type V DES, which are introduced in Chapter 4.

Paper II exploits the hydrophobic nature of Type V DES, allowing them to form the dispersed phase in an oil in water emulsion system. However, emulsions are naturally unstable, due to many unfavourable interactions between the hydrophobic and hydrophilic (aqueous) phases. Therefore, once formed, these emulsions are energetically disposed to breaking down into their constituent parts. In Chapter 5, the making, breaking and stabilisation of emulsions is briefly described. Within Paper II, poloxamer surfactants are used to stabilise the interface of the DES emulsions. In Chapter 6, the interactions and common surfactants are discussed to provide context for Paper II.

Paper III: Gelation of 12-Hydroxystearic Acid in Type V Eutectic Solvents

Furthering the work into the tunable nature of Type V DES, as mentioned in Chapter 4, this paper discusses the work undertaken into exploring the 'designer' solvent properties of 25 binary type V eutectic solvent (ES) mixtures. Due to the varying ES properties, arising from to the varying components used at different stoichiometries, the solvent environment can be varied. This changing solvent environment affects the gelation of a low molecular weight gelator (LMWG), 12-hydroxystearic acid (HSA) which are introduced in Chapter 6, Section 7, which forms through a hydrogen bonding network of gelator molecules which entraps the solvent within. Gels are curious materials, which sit on the boundary between both liquids and solids, therefore featuring properties of both. Simple 'inversion' tests can allow a sample to confirmed whether it flows or not, and hence is not a liquid, but the application of rheological methods allow a quantitative measure of the gel structure, which is discussed in Chapter 2.

Gelation and Design

This thesis is entitled *Gelation By Design*, as all three manuscripts within are unified by the concept of gelation and a degree of design; In Paper I, a microfluidic device was designed and built for dedicated use of observing aluminium gels during synchrotron small angle scattering experiments. Aluminium salts react with the model protein BSA, forming protein gels which model those forming in our underarms on the application of an antiperspirant. In the Paper II, the surfactant phase on the emulsion surface is modified by the addition of stearate salts, forming a compacted gel-like phase on the addition of a sodium salt which improves the emulsion stability. In Paper III, eutectogels of varying characteristics are formed through the entrapment of ES mixtures within fibre networks of the LMWG HSA. In Papers II and III, eutectic solvents are used which allows them to act as designer solvents, which can be tuned to a certain application. Especially in Paper III, the solvent componentry and their stoichiometries are exchanged to control or 'design' the solvent environment and therefore the formation of HSA fibres within.

Chapter 1

Scattering Methods

1 Small Angle Scattering Theory

Small Angle scattering (SAS) is a technique which observes the diffraction (scattering) of X-rays and neutrons at angles of ≤ 10 °. This diffraction is caused by the radiation in question passing through two mediums with a difference in scattering length density (SLD). In X-ray scattering, this difference arises due to variable electron densities of the electron clouds of atoms, whereas neutrons are scattered by interacting with the nucleus of the atom. Despite the fact that neutrons and X-rays have similar wavelength range, the differences between the X-ray and neutron atomic scattering lengths allows for a valuable contrast between the two methods. Neutron scattering is much slower, more expensive to conduct and more safety aspects must be considered, but the availability of alternative scattering lengths arising from the nuclear interaction make it is a valuable method nonetheless.

Small angle scattering is useful as the patterns collected can be used to interpret the size, shape, morphology and structure of sample species with feature lengths on the nanometre/ångström scale. This allows us as scatterers to gain understanding of many systems including micelles, nanoparticles, polymers, aggregates and gels. The fundamentals are well known and although introduced here, more in depth approaches can be found in the literature. [1–3]

1.1 Scattering Length Densities

As the scattering of X-rays originate due to interactions with an atoms diffuse electron cloud, the X-ray scattering length is directly related to its atomic number (Z). This scattering length can be calculated according to Equation 1.1, where b_c is the bound coherent scattering length and r_e is the classical electron radius (2.81 $\times 10^{-13}$ cm).

$$b_c = Zr_e \tag{1.1}$$

However, as neutrons are scattered by the nucleus rather than the electron cloud, the scattering lengths of isotopes vary greatly from X-rays. The magnitude of scattering of neutrons with a given isotope is not determinable theoretically, as it arises due to complex potential energy interactions and nuclear resonance fields within the nucleus. Therefore these values must be determined experimentally, for each commonly used isotope.[4]

The seemingly random variation in scattering length, is the reason why conducting neutron scattering experiments is worthwhile. Light elements such as hydrogen, due to their low atomic mass, feature very small X-ray scattering lengths and are practically invisible during SAXS experiments. However, different isotopes of the same element can feature vastly different neutron scattering cross sections. The classic case is hydrogen and deuterium, which scattering lengths are -3.74 fm and 6.67 fm respectively. The X-ray and neutron atomic scattering lengths for some common isotopes are shown in Figure 1.1, for visual comparison.

In order to compare the scattering length *density* of different materials. Their physical properties must also be taken into account. To calculate their scattering length density (ρ), the molecular volume (V_m) must be considered, which is calculated according to Equation 1.2, where the molecular mass (M) and mass density (ρ_m) of the material must be known.

$$V_m = \frac{M}{\rho_m N_a} \tag{1.2}$$

ρ) is calculated as in equation 1.3, by summing all of the bound coherent scattering lengths (b_i) of n atoms within a molecule of volume V_m. The stoichiometry of multiple occurrences of the same element must be accounted for when summing up the scattering length contributions, this can be done according to the relative concentrations or stoichiometric values in the chemical formula.

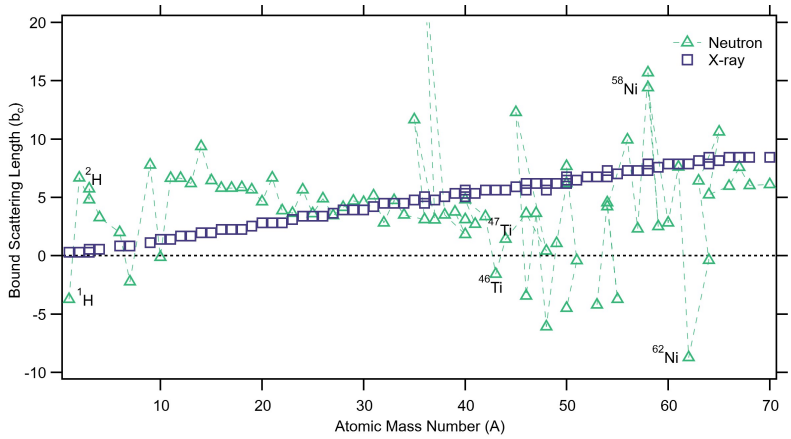

Figure 1.1: The varying scattering lengths (b_c) vs. atomic mass number for X-rays and neutrons, values as reported by V.F. Sears (1992).[4]

$$\rho = \frac{\sum_{i=1}^{n} b_c}{V_m} \tag{1.3}$$

For example, this can be used to calculate the ρ of H_2O and D_2O, which feature neutron scattering length densities of -0.561 and 6.331 $\times$ 10^{-6}Å^{-2} respectively.

When conducting a scattering experiment, it is key to ensure that there is a difference in ρ between the sample and background (i.e. solvent system). This is of more concern in SANS experiments due to the practically random variation in scattering length with atomic number, meaning that the SLD of a material cannot be calculated without knowledge of the isotopes it contains. If the ρ of the sample and solvent are equal, no scattering features other than the incoherent background will be observed. However, this can also be highly useful in SANS experiments, where components in the system can be 'contrast matched' to reduce the scattering contributions from a specific component in the sample to zero. This is commonly achieved using a combination of H_2O and D_2O to vary the contrast between components, which, for example, allows the core or shell of nanoparticles to be viewed in isolation of one another. This is allowed due to the largely different scattering lengths of hydrogen and deuterium whilst these isotopes have practically indistinguishable chemical properties. This method can be employed to observe different parts of micelles,[5, 6] surfactant head groups/tails,[7] hydration shells[8] amongst a myriad of other systems and features. This was first accomplished in SANS in the 1970s to observe the structure of polymer coils.[9]

This is illustrated in Figure 1.2, the differing ρ of the solvent (yellow, in the

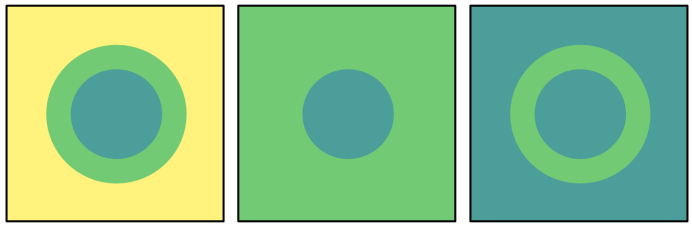

Figure 1.2: Illustration of how varying the solvent ρ, (here shown where SLD is represented by colour) can highlight parts of a core-shell particle. The core and shell remains the same, but the solvent can be matched to them individually, making them indistinguishable from the solvent.

left hand side image) and a biphasic system (green and blue) is illustrated. By altering the ρ of the solvent, it can be 'contrast matched' to the ρ of the core or shell of the particle, when this occurs there is no difference between the scattering from the solvent and that component of the system, allowing the other component in the system to be observed independently.

1.2 A Basic Scattering Event

Max von Laue was the first to discover that X-rays could be used to elucidate crystal structures of copper sulphate crystals in the first X-ray diffraction experiments in 1912, after he realised he needed to use a radiation with a wavelength on a similar length scale to the interatomic distances of the crystals in question.[10] It wasn't until 1930 where the first mention of small angle X-ray scattering was made by Krishnamurti, who observed 'strong scattering at small-angles' when looking into the structures of amorphous carbon samples.[11] As beamlines with higher fluxes become more common, with longer sample-detector distances, smaller scattering angles and therefore larger feature lengths are increasingly more accessible. Today, up to micron scale features can be observed at the smallest angles accessible with the current technology.[12]

As the radiation is scattered through the sample, the radiation is detected and recorded on the detector. The momentum transfer vector (q), shown in Figure 1.3 is a measure of the degree of scattering and has the units of inverse distance (typically $\mathring{A}^{-1}$). This allows measurements taken on all small angle scattering instruments to be directly compared, as the measurement is independent of the wavelength of radiation used. For high quality scattering data, the radiation used must have a well-defined wavelength or wavelength band. This allows the q vector to be clearly defined for each scattering event.

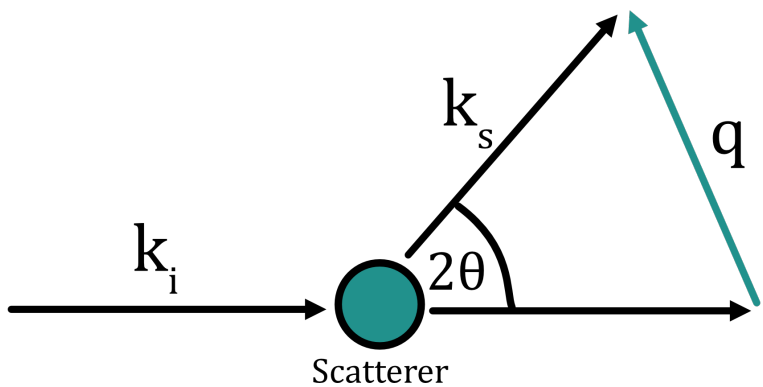

Figure 1.3: Illustration of q (momentum transfer) vector in a simple scattering experiment, where 2θ is the scattering angle and k_i and k_s are the incident and scattered photon energies.

2 Elastic Scattering

Elastic scattering occurs when the magnitude of momentum is preserved during a scattering event. This allows the scattering vector q to be calculated, if the incident and scattered energies are known, as seen in Equation 1.4

$$q = k_s - k_i \tag{1.4}$$

Where k_i is the incident energy, k_s, is the scattered energy and q is the momentum transfer.

$$q = (4\pi/\lambda)sin\theta \tag{1.5}$$

Using Equation 1.5, which is applicable to both SAXS and SANS, using the wavelength of the incident radiation, and the scattering angle 2θ, q can be determined over the range of angles which the sample scatters. This can then be substituted into Equation 1.6 below, which allows the separation distance of scattering centres to be calculated.

$$q = 2\pi/d \tag{1.6}$$

In a sample where Bragg peaks are present in the scattering pattern, the Bragg equation (Equation 1.7) can be used to determine the d-spacing in the sample. This information can be used to elucidate crystal structure and is commonly used in powder and single crystal diffraction.

$$n\lambda = 2dsin\theta \tag{1.7}$$

A fundamental observation of these equations is that at larger q value, smaller d spacings can be observed, with the extreme case of this used in X-ray diffraction for interatomic distances and crystallography down to the ångström (Å) distance scale. At the other extreme some synchrotron beamlines are capable of observing up to micron sized features using USAXS, at the smallest scattering angles.[13] This is extreme of the technique is made possible by using beamlines of the maximum possible length to accommodate the divergence of the narrow scattering angle, but implementing such measures are expensive due to the large beamline footprint and premium cost associated with this in research facilities.

As discussed in Section 1.1, in order for scattering to be observed, the sample must feature a difference in scattering length density (ρ) between the material and its solvent. Any given particle has the scattering length distribution $\rho(r)$, which contains all of the contributions from all of the time-preserved correlated distances between atomic positions within the particle volume. To observe the scattering contributions from the particle in isolation of its bulk solvent, the solvent length density (ρ_s) can be recorded separately and subtracted from the scattering signal of the combination, as in Equation 1.8.

$$\Delta\rho(r) = \rho(r) - \rho_s \tag{1.8}$$

This difference in the signal is known as the excess scattering length density, its average can be taken, as shown in Equation 1.9. If the scattering length density of the solvent and the particle are the same, $\Delta\rho \approx 0$ and very little scattering will be observed.

$$\Delta\rho = \langle\Delta\rho(r)\rangle \tag{1.9}$$

Once solvent scattering contributions are removed from the scattering profile, the isotropic scattering can be described by the absolute square of the Fourier transform of $\Delta\rho$(r) taken over the scattering volume V.

$$I(q) = \frac{1}{V}\Big|\int_V \Delta\rho(r)exp(iq.r)dr\Big|^2 \tag{1.10}$$

However, when the particles are identical, free to tumble in solution, the scattering intensity only depends on the magnitude of q, allowing Equation 1.10 to be simplified to Equation 1.11, where n = no. density of particles and V = particle volume.

$$I(q) = n\Delta\rho^2V^2P(q)S(q) \tag{1.11}$$

The scattering may be viewed as a manifestation of the scattering amplitudes from each individual scattering centre, which constructively and de-constructively interfere to generate a the scattering pattern observed. These scattering amplitudes cannot be directly observed experimentally, but the square of this (the scattering intensities) can, wherein the information about the size, shape and contrast of the particles are encoded in the form of their structure factor and form factors. $S(q)$ in Equation 1.11 is the structure factor, which describes the

interferences between neighbouring particles in the sample. In dilute samples, where the particles are too dilutely dispersed to interact directly with each other, the structure factor = 1 and the only scattering contributions come from the form factor ($P(q)$) as a product of the volume and contrast of the particles in the sample. The rotationally average form factor ($P(q)$) can therefore be expressed as in Equation 1.12.

$$P(q) = \frac{1}{V^2}\left\langle \left| \int_V exp(iq.r)dr \right|^2 \right\rangle \tag{1.12}$$

3 Sources of Radiation

By increasing the flux of a SAS instrument, scattering patterns can be collected with better statistics (as the certainty of a result is related to the square root of the number of measurements taken), in shorter time frames and less strongly scattering samples can also be measured. The bottleneck for increasing the flux in a laboratory scale instrument is the heat generated from bombarding a stationary metal target. This issue can be reduced through the use of spinning plate targets to increase the surface area of the bombarded target and more recently the flux can be further increased through the use of liquid gallium targets, which allow much greater heat dispersal and therefore allow access to greater magnitudes of flux. However, the collection times for even the strongest laboratory scale instruments is on the time frame of minutes for strongly scattering samples. If the desired experiment requires large amounts of samples to be measured, or at rapid time resolution frames, a dedicated synchrotron facility must be used.

$$\nu = c/\lambda \tag{1.13}$$

$$E = eV = h\nu = hc/\lambda \tag{1.14}$$

These equations can be used to calculate the wavelength of an X-ray photon from the its frequency and how the units of electron volts, energy and wavelength can be used interchangeably.

3.1 Lab X-ray Sources

X-rays can simply produced by bombarding a metal target such as copper or molybdenum with electrons. This can be performed by an electron gun, which is essentially a piece of wire, which emits electrons due to thermionic emission. These electrons are then accelerated using a potential difference (in vacuum) towards a target, which removes an electron in the target's inner electron shell. This causes a cascade of electrons to fill the vacant energy levels and hence the energy change is released by a characteristic X-ray photon as seen in Figure 1.4.[14] The most commonly used copper radiation is CuK_α radiation, of which the photons have a wavelength 1.54 Å.

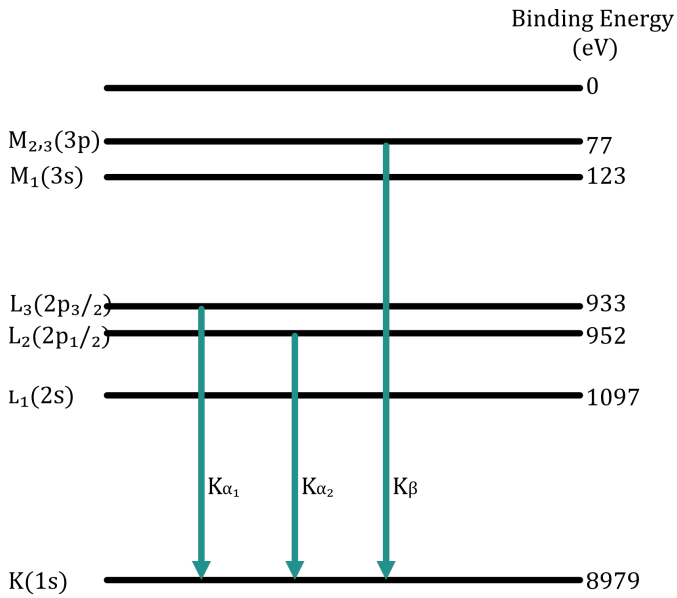

Figure 1.4: A schematic illustrating the binding energies of Copper, values taken from the 'X-ray Data Booklet', Lawrence Berkeley National Laboratory. [15]

In some texts, electron volts and wavelength are used interchangeably, this is due to different conventions of quantifying the same thing, and they can simply be converted between. When regarding to the energy of a photon, this can be expressed in eV to avoid the cumbersomely small quantities if the energy was to be stated in joules. For the same reason, the wavelength of the particle can also be stated, as when conducting scattering experiments, this is of more use.

3.2 Synchrotron X-ray Sources

Synchrotron radiation allows much broader sample environments due to the higher fluxes available with this method of photon production. This allows more signal to noise ratio and therefore the necessity of vacuum is not necessary at the sample position. This in itself allows a plethora of experiments to be carried out which otherwise would not be possible. The q range of these instruments is also much greater, such as the I22 beamline (Diamond Light Source, UK) which is depicted in Figure 1.5. This beamline has a q range of 0.0011 - 9.45 $Å^{-1}$, using the full sample-detector distance (SDD) of 9.9 m and simultaneous collection of SAXS and WAXS data. With purpose built beamlines, greater SDD are available which allow the measurement of scattering at increasingly low q values, the above example able to resolve real space distances of up between 1 Å almost up to 1 µm .

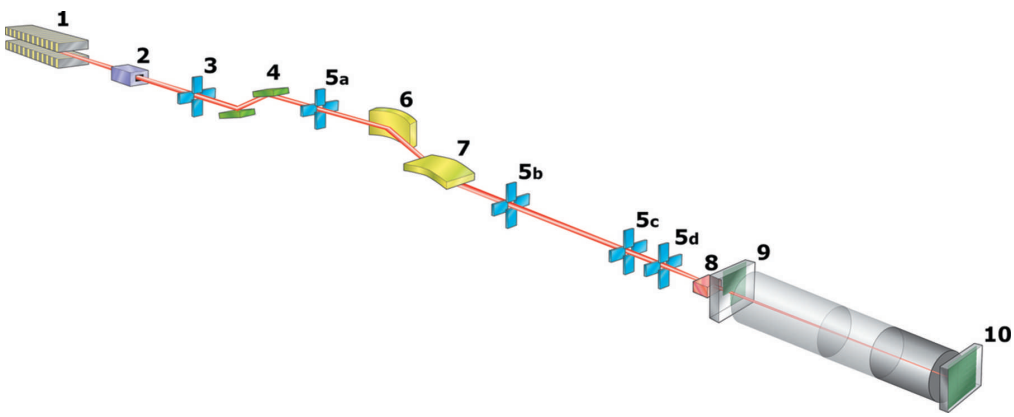

Figure 1.5: A schematic of a synchrotron SAXS beamline (I22 - The Diamond Light Source, UK). Reused with permission (CC-BY)[16]

3.3 Neutron Spallation

Compared to fission, producing neutrons via spallation is much safer as the process can be stopped immediately in the event of an emergency. However, where nuclear fission produces energy and excess neutrons, spallation sources require large amounts of continuous energy input to do so. This large amount of energy is used to accelerate protons towards a metal target, normally consisting of tungsten, liberating the neutrons which are used for analysis. These neutrons are produced in timed pulses, which allows exact measurement of the time of production of the neutrons to be known. Knowing the time of production is of paramount importance when carrying out scattering experiments, as the speed (and therefore wavelength) of the neutrons must be known in order to calculate their momentum transfer (q) for scattering analysis.

The De Broglie equation makes the link between the momentum of a relativistic particle and its wavelength, it can be used to calculate the wavelength (λ) of a neutron, as in Equation 1.15.

$$\lambda = \frac{h}{p} \tag{1.15}$$

However in order to calculate the momentum of the neutron, its speed (v) must be known. As mentioned, the neutron is a relativistic particle, meaning that its kinetic energy can be directly calculated in Equation 1.18.

$$p = m_n v \tag{1.16}$$

Substituting $p = m_n v$ into Equation 1.15 gives:

$$\lambda = \frac{h}{m_n v} \tag{1.17}$$

As the neutron is a relativistic particle, its kinetic energy (E) is calculated as in Equation 1.18.

$$E = \frac{1}{2} m_n v^2 \tag{1.18}$$

Kinetic energy can also be expressed in terms of momentum (p), as in Equation 1.19.

$$E = \frac{p^2}{2m} \tag{1.19}$$

Substituting $p = \frac{h}{\lambda}$ from Equation 1.15 gives the relationship between the kinetic energy of the neutron and its wavelength in Equation 1.20.

$$E = \frac{(\frac{h^2}{\lambda^2})}{2m_n} = \frac{h^2}{2m_n\lambda^2} \tag{1.20}$$

As the kinetic energy of a particle is related to its absolute temperature, Equation 1.21 can be used to calculate this:

$$\langle E \rangle = \frac{1}{2}m\langle v^2 \rangle = \frac{3}{2}K_B T \tag{1.21}$$

Where the average energy $\langle E \rangle$ is related to the average velocity $\langle v \rangle$ of particles of gas, K_B is Boltzmann's constant (1.381×10^{-23} and T is the absolute temperature.

As an approximation, this is often simplified to:

$$E = K_B T \tag{1.22}$$

This energy value (E) can then be used to calculate the neutron wavelength using Equation 1.23.

$$\lambda = \sqrt{\frac{h^2}{2m_n E}} \tag{1.23}$$

Therefore, by altering a neutrons temperature (kinetic energy) through modulation, the neutrons wavelength is controlled. This is achieved by introducing the neutrons to temperature controlled modulators such as liquid water or liquid hydrogen, where the neutrons equilibrate with their environment. In texts, neutrons can be referred to as 'cold', 'thermal', 'hot' etc. and this is a colloquial way of using their temperature by way of describing their approximate wavelength. For SANS measurements, cold neutrons tend to be used. For example, a commonly used SANS instrument, SANS2D (ISIS, UK) uses cold neutrons modulated to approximately 25 K with a wavelength range of 1.75 - 16.5 Å.[17]

Chapter 2

Aluminium Salts and Antiperspirancy

An antiperspirant is a product which, when applied to the skin, reduces perspiration. For the majority of the last century, aluminium salts have been extensively used as the only known effective active ingredient in antiperspirants. These salts are potent, affordable and available in a great range of products across the globe. These products include the familiar aerosol sprays, emulsions, roll-ons, solid sticks, and aqueous solutions to suit a range of personal needs and preferences.

1 Antiperspirancy

Although the effectiveness of aluminium salts has been known for many decades, the exact process by which they function is not fully known. This has lead to many theories and proposed models by which these salts function. One thing all theories agree on is that the eccrine gland is the target gland for antiperspirants, which produces the aqueous solution most commonly associated with sweating.

In 1977, 'Plug Theory' was proposed by Reller and Leuders, and it suggested the build-up of insoluble aluminium salts in the eccrine sweat gland, forming a gel 'plug' to physically prevent sweating.[18] A few studies into the effects of aluminium chloride were carried out in the 1980s, although these were simple experiments, they unveiled some key findings which are still relevant today. Quatrale et al. compared ACH, $AlCl_3$ and AZAG antiperspirants in the 1980s in 'Tape

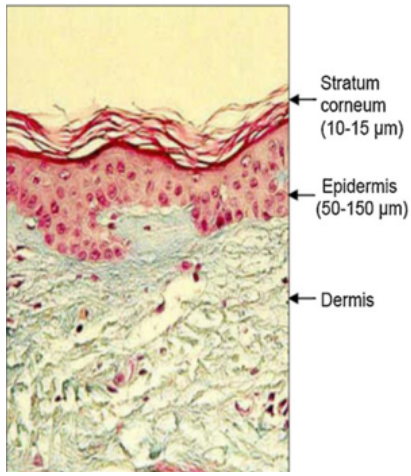

Figure 2.1: The structure of the stratum corneum, epidermis and dermis layers of the skin, reprinted with permission from Menon et al. [20]

stripping' experiments which used adhesive tape to remove the top layers of the skin, reinvigorating sweating after the application of antiperspirant salts. The volume of sweat produced was compared before and after stripping.[19] This study showed that $AlCl_3$ penetrates deeper into the skin, below the stratum corneum, suggesting that the increased depth of 'plug' caused the increased efficacy in $AlCl_3$. The ACH and AZAG formulations were found to penetrate to a lesser degree and therefore could be removed along with the stratum corneum (top) layer of the skin, indicating that the 'plugs' penetrated the skin to a depth less than 25-35 µm below skin surface. It has been suggested by many, that the depth of the gel plug in the skin is related to the pore-plugging capability, however as superior antiperspirant action is noted with zirconium salts (compared to ACH), despite both of these salts only penetrating the skin to the stratum corneum. These observations support the hypothesis that there are multiple methods employed by aluminium salts to prevent sweating.

In 1984, Holzle et al. studied the effects of $AlCl_3$ on individuals suffering with hyperhydrosis.[21] No effects were observed to the structure of the apocrine gland, but it was noticed that the structure of the eccrine gland was degraded due to the eccrine gland becoming blocked by the aluminium salt, causing a build-up of pressure in the gland which causes 'dilation and atrophy of the eccrine acini'. This dilation and atrophy can be seen through histological examinations, although a correlation could not be drawn to the amount of exposure (through treatment) of $AlCl_3$ and the extent of structural change to the eccrine glands in individual cases.

The 'occlusive plug theory' is the most common antiperspirant theory today, which assumes that the aluminium salts travel up the eccrine sweat pore and on reaction with the proteins present on the keratinised eccrine gland walls and in produced sweat, an aluminium based gel forms, physically blocking the pore.[22–24] This work is discussed in more detail in Chapter 3.3.

Regardless of the theory for pore plugging, the aluminium salts are thought to react with naturally occurring skin/sweat proteins due to their positive charge. Generally speaking, the greater the charge density on the ion, the more interaction with the protein and the greater antiperspirancy effect. In the following section, the differences between the commonly used aluminium antiperspirants are discussed.

2 Aluminium Salts

2.1 $AlCl_3$

Aluminium chloride ($AlCl_3$) was the first known antiperspirant, discovered by Stillians in 1916.[25] This was applied using absorbent cotton in a 25% aqueous solution every 2-3 days to provide relief from perspiration. The first use of this was not intended for underarm application but to keep hands dry when carrying out delicate tasks such as surgical operations. However, through successful advertisement campaigns, the use of antiperspirant to tackle body odour soon boomed in popularity.

$AlCl_3$ solution can be simply produced by reacting aluminium metal with hydrochloric acid, with dilution to the required concentration. Despite its efficacy, this aluminium salt is not user friendly due to its highly acidic nature, which causes severe skin irritation and damage to clothing. Nowadays, $AlCl_3$ is only used where absolutely necessary, in extreme cases of hyperhydrosis, due to its superior antiperspirant efficacy compared to other aluminium salts.

2.2 ACH

To allow for more user friendly alternatives to $AlCl_3$, the salt can be partially neutralised with a base such as sodium carbonate. This yields aluminium chlorohydrate (ACH) salts, which due to reduced acidic character, is both less damaging to the skin and clothes whilst maintaining a degree of antiperspirant efficacy. In 1947, ACH was introduced as a more convenient alternative to $AlCl_3$

and was patented in 1949.[26] ACH is known by its neutral general formula of $Al_2(OH)_5Cl$, however this formula encompasses multiple structures containing varying amounts of Al, O, H and Cl.[27–29] These structures compose of a complex mixture of aluminium polycations which firstly depends on the degree of hydrolysis of the aluminium cation, ranging from the unhydrolysed $[Al(OH_2)_6]^{3+}$ hydrate to the insoluble and completely hydrolysed $Al(OH)_3$. The properties of the common polycation aluminium chlorohydrate species are shown in Table 2.1.

Table 2.1: Properties of various aluminium polyoxocations and their hydrolysis ratios. [30]

Al structure	No. of Al	Hydrolysis ratio
$[Al(H_2O)_6]^{3+}(aq)$	Al_1	0
$[Al_2(OH)_2(H_2O)_8]^{4+}(aq)$	AL_2	1
$[AlO_4Al_{12}(OH)_{24}(H_2O)_{12}]^{7+}(aq)$	Al_{13}	2.46
$[Al_2O_8Al_{28}(OH)_{56}(H_2O)_{26}]^{18+}(aq)$	Al_{30}	2.40
$Al(OH)_3(s)$	Al_1	3
$[Al(OH)_4]^-(aq)$	Al_1	4

The overall hydrolysis reaction is as seen below in Equation 2.1. [31–34] Under basic conditions, the released H_3O^+ is consumed by the OH^- ions in solution, which drives the reaction to further hydrolysed aluminium salts.

$$[Al(OH_2)_6]^{3+} + hH_2O \rightleftharpoons [Al(OH)_hOH_{2_{6-h}}]^{(3-h)} + hH_3O^+ \qquad (2.1)$$

If the concentration ratio of $[Al^{3+}]$:$[OH^-]$ is $1:2.46$, the $[AlO_4Al_{12}(OH)_{24}(H_2O)_{12}]^{7+}$ (Al_{13}) ion forms as a major product.[35] This ion is desirable for antiperspirant products due to its increased efficacy compared to the other polycations, due to its high charge to radius ratio. This allows greater electrostatic interactions with negatively charged protein residues, yielding a stronger antiperspirant effect.[19] The Al_{13} ion exists with a central AlO_4 with a tetrahedral structure, with twelve AlO_6 octahedral groups surrounding this, and are known as Keggin isomers,[36] as shown in Figure 2.2.[37] This structure is believed to manifest due to the localised high pH conditions caused by the production of hydroxide ions formed at the aluminium ion surface, which is diminished as the reaction continues, allowing the octahedral aluminate to form under the bulk low pH conditions.[27]

2.3 AACH

As the Al_{13} polycation is desirable for use in antiperspirant products, raising its proportion in the polycation composition allows for increased potency

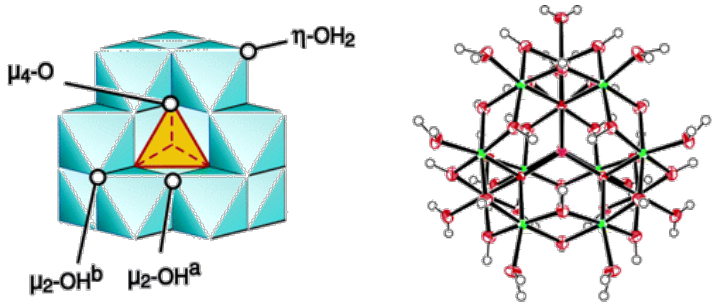

Figure 2.2: The Al_{13} Keggin ion, reprinted with permission from Casey at al. [37]

products. This is achieved by heating a dilute aqueous solution of ACH, which causes the proportion of the Al_{13} isomer to increase in solution. This polycation distribution can be 'locked in' by spray drying the solution, which rapidly removes the water and preserves its composition. The product of this process is called 'activated' aluminium chlorohydrate (AACH).[38] The increased proportion of Al_{13} has been shown using size exclusion chromatography and capillary electrophoreses.[30, 39]

However, when left in aqueous solution, AACH rapidly equilibrates back to its previous distribution and reverts back to ACH, as the (Al_{13}) concentration is depleted once more. This degradation is likely due to the formation of larger aluminium polycations, such as Al_{30},[40], with lower charge density and therefore lower antiperspirant efficacy. In consumer products, the polycation distribution and the related efficacy is maintained by storing these salts in anhydrous environments, such as as a suspension in a low viscosity oil for aerosols or oil-based sticks.

2.4 Zirconium Salts

The combination of zirconium salts with aluminium chlorohydrate increases antiperspirant efficacy in comparison to aluminium chlorohydrate alone, due to the high charge on the Zr^{4+} ion and has been included in antiperspirant products since the 1970's. These products typically contain zirconyl chloride and are commonly named aluminium zirconium chlorohydrex glycine (AZAG/AZG/ZAG).[41–43] The glycine component acts as a buffer to the zirconium by complexing its carboxyl group to the positive zirconium ions, which also bridges other zirconium cations or oxo-aluminium ions through hydrogen bonding its positively charged, protonated amino group. Pan et al. have used zeta potential measurements to quantify the charge-neutralisation capability of antiperspirant salts

and saw that less than half the quantity of a zirconium chloride salt was needed to reach the IEP of BSA compared to AACH alone, which is attributed to its superior antiperspirant performance.[38] However, zirconium salts are limited in their use for aerosol products as its particulates can be damaging to the respiratory system.[44] Therefore, these salts are limited to products such as sticks and roll-ons.

Chapter 3

Microfluidics

Microfluidics is a method which employs reaction vessels which feature at least one micrometre length scale dimension, which operates under a continuous flow regime. Microfluidics can be used in a plethora of different applications to recreate physical and chemical environments in highly flexible and adaptable ways. The main advantage of this method is that the sample environment is much smaller than would be possible to use in a traditional laboratory glassware scale, allowing specific sample environments to be modelled and represented at a higher degree of specificity. As microfluidics also embrace a 'continuous' method rather than a 'batch' method, the environmental conditions can be adapted in real time, allowing a greater experimental volume to be covered. Microfluidic reaction chambers can also be designed to be adaptable so that they can be modified to feature a plethora of synthesis or analysis methods. This can allow for many coupled *in situ* methods such as UV or IR spectroscopy, liquid chromatography, or as is discussed in the Paper I in this thesis; *in situ* small angle X-ray scattering (SAXS).

1 PDMS Microfluidics

Polydimethyl siloxane (PDMS) is a polymer, which can be cast into a mould and cured. This is the most common material used for the production for tailor-made microfluidics as it is very quick, cheap and simple to produce large amounts of microfluidic devices. Depending on the precision required, moulds can be produced through a multitude of methods, including computer aided milling of plastics, 3D printing and if high precision is required; soft lithography. Once a

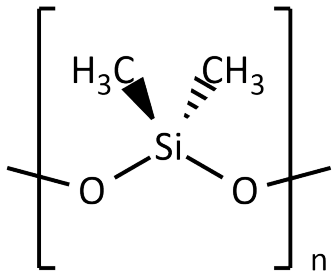

Figure 3.1: The siloxane monomer of a PDMS polymer

mould has been produced, it can be used indefinitely. PDMS allows microfluidic devices to be produced at low cost with relative ease. This method allows for a great deal of adaptability such as the addition of electrical sensors.[45] Due to its optically transparent nature, devices produced from it can be simple observed under a microscope.

The casting process of these devices is a simple process of preparing the polymer, degassing via vacuum, casting and finally baking the polymer, as seen in Figure 3.3. Once the PDMS has set, it can be ablated in an O_2 plasma chamber and therefore permanently bonded to a glass substrate due to the removal of methyl groups via ablation, exposing Si-O bonds which can covalently bond to a clean glass substrate. This step is crucial to ensuring the device is water-tight, but also affects the surface chemistry of the device, which affects how the fluids interact with it. As the plasma ablation causes the surface to feature a high density of Si-OH bonds, as illustrated in Figure 3.2. These exposed bonds cause the PDMS surface to be hydrophilic. As the PDMS ages, the surface relaxes as the methyl groups migrate back to the surface and becomes less hydrophilic once more.

This variable surface charge also impacts how surface active species such as proteins interact with the channel walls, as there are charged amino acid residues on proteins.[46] Therefore, they adhere to this similarly to how they would interact with a keratinised skin layer in the eccrine sweat gland, making this type of microfluidic device a good candidate for observing the formation of occlusive plugs of antiperspirant salts with sweat proteins, as seen in Figure 3.4.

However, although these microfluidics are suitable for observing reactions under optical microscopy, if X-rays are the probing radiation of choice, they are no longer suitable. Due to their construction of a glass substrate and several millimetres of PDMS required to make a rigid device, a large proportion of X-rays are absorbed by the microfluidic device itself. Therefore, for SAXS experiments,

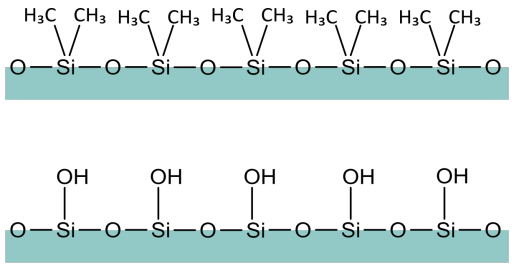

Figure 3.2: The PDMS polymer, before (above) and after (below) O_2 plasma treatment

another approach is required, which is discussed in the following section.

2 Multi-layered Microfluidics

Producing multi-layered microfluidic devices requires the combination of many components to work in harmony, rather than a fused complete unit as in PDMS microfluidics.[47, 48] Due to the design of the device, sample holders can be custom made, e.g. for mounting on a beamline, which can allow the parts of the device in the X-ray beam to feature much lower absorption compared to glass or PDMS devices. In Paper I, the design included milled HPLC ports to in the chassis of the device, which allowed high quality fluidic connections to the device and therefore reliable fluid flow. Due to the multi-layered design, this design allows for more tailorability to experimental conditions, where the channel dimensions could be changed simply by exchanging one of the layers when assembling the device. If other environmental control were required, such as temperature control, it would be rather simple to implement, if machined out of a conductive material such as steel or aluminium.

3 Aluminium Gels Observed within Microfluidics

In the last decade, another research group used modern physical chemistry methods and mathematical modelling in an attempt to reveal the pore blocking mechanism of ACH.[22] The basis of this work began with using PDMS microfluidic devices, produced via a soft lithography mould, which can be used to produce microscopic microfluidic structures with a resolution of 1 µm. This device was then used to cast PDMS microfluidic devices which could be plasma bonded onto glass slides. These chips featured an ACH channel which acted as a reservoir of the AP active (15% w/w) and an orthogonal sweat channel, which had a width

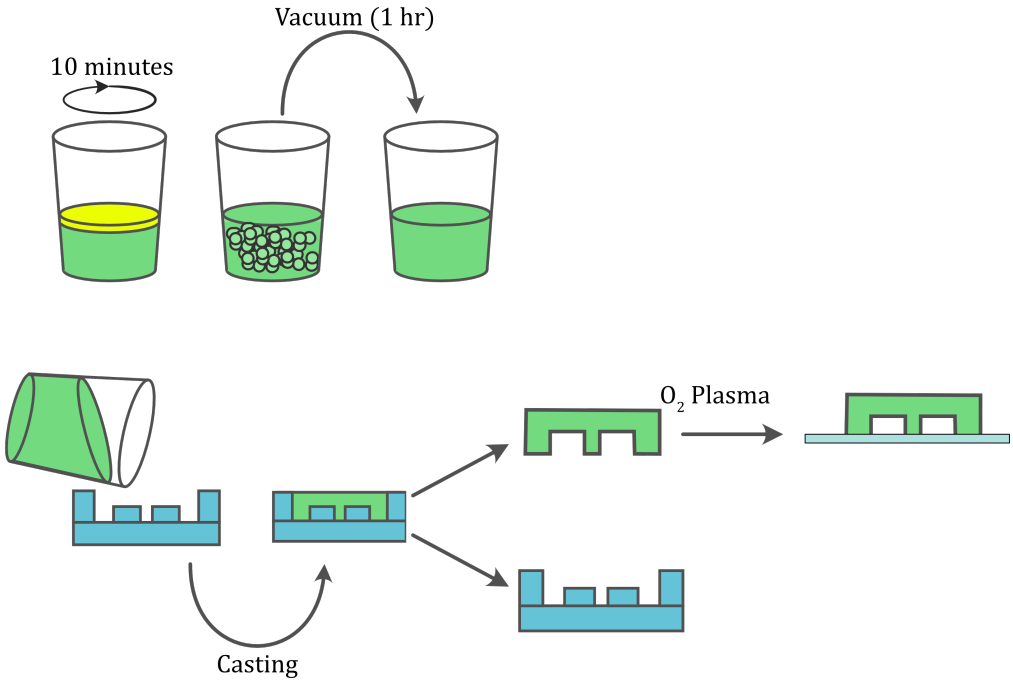

Figure 3.3: The process of preparing PDMS devices, where the PDMS must be combined with a curing agent, mixed thoroughly, degassed under vacuum for one hour, cast into moulds, baked and plasma treated to permanently bond to a glass substrate.

and height of 50 µm and 55 µm respectively in order to mimic a physiological eccrine sweat gland. For SAXS measurements, larger channel widths were used, with an ACH channel width of 800 µm and sweat channel of 300 µm) to allow for accurate measurements and more repeatable results. The increase in the size of the chip meant that the joining fluid menisci had lower Laplace pressures causing more repeatable plug locations within the microfluidic device, which was essential for the beamline experiments. Gel plug formation was studied using SAXS, although only median q range data was available due to instrument limitations, but this provided information of the relative concentrations of the BSA protein and aluminium aggregates. This initial study by the group suggested that as PDMS is capable of adsorbing proteins, this facilitates nucleation of the gel plug from the walls to the centre of the channel.

Subsequently, the group published another paper,[24] building on their previous findings. In this work they further explored the mechanism of plug formation and confirmed that aluminium polycations react electrostatically with the negatively charged glycine and aspartic acid residues which feature in BSA to form aggregates. It was found that no gel plug formed in the sweat channel of the previously mentioned PDMS 'chip' when the artificial sweat pH was below 4.7,

which is the isoelectric point (IEP) of BSA. The IEP is known as the point where there is net zero electrostatic repulsive forces between the protein and the polycation. As the pH increased above this value the gel plug density was shown to become much denser, up to pH 9, where a considerable difference was observed in plug density, due to the increase in magnitude of attraction between the protein residues and the aluminium polycation. The group also varied the concentration of ACH delivered by the ACH channel between 1-15% and found that the plug location got much closer to the channel junction at lower concentrations and the gel plug became much more superficial under these conditions.

Interestingly, if NaCl was removed from the artificial sweat solution, no gel plug formed. It was postulated that this was due to the screening effect of the ions, which prevent the repulsion between the positive Al ion and residues on BSA. It was noted that if lactic acid and urea were absent from the artificial sweat mixture, the plug was formed much deeper into the sweat channel. It has been reported that lactic acid hydrolyses the Al polycations into monomers and dimers and chelates with these newly formed species. This may be the reason why lactic acid is a key component in sweat, causing facile formation of the gel plugs.[49] Urea increases the rate of gelation of BSA, by unfolding the protein in solution, and denaturing its tertiary and secondary structures.[50]

This study also used confocal microscopy to gain understanding of the plug formation and discovered that the BSA-FITC (fluorescent analogue of BSA) coated the channel walls, supporting that the gel nucleates at the channel walls and develops inwards to form the gel plug. This is thought to be similar to the mechanism of pore plugging in physiological sweat pores, due to the keratinised upper layer which lines the sweat pore having oligosaccharide chains covalently attached to amino acid side chains, which are capable of interacting with the aluminium polycations in order to facilitate nucleation at this site. Further work by this group was published in 2021, and researches the in-depth process of gel-plug formation in the PDMS microfluidic devices.[23] This group has used SAXS to probe the plug formation in their first publication on this topic, but only achieved basic measurements which indicated a relative amount of gel forming over a period of time. It would be informative to do more in-depth studies into the mechanisms of gel plug formation to identify the relationship that the aluminium polyoxocations have with the protein in forming the aggregates. An improvement to the microfluidic design in these experiments would have been to match the flow mechanics to physiological conditions, as sweating is known to occur in a pulsing flow, which may produce a more convincing model of the sweat gland.[51]

4 A Microfluidic Device for *in situ* SAXS

Within this thesis, Paper I discusses the steps taken towards furthering the knowledge of aluminium salts in a model eccrine environment. This is accomplished by producing a multi-layered microfluidic device, capable of high X-ray transmission, to allow a fast acquisition of high quality SAXS data, in an attempt to view the formation of aluminium gel plugs inside the model environment in real time.

However, this work began with producing and using PDMS-glass microfluidics in the lab, which are shown in use in Figure 3.4. This step was completed to replicate the previous works in the literature, whilst designing and producing the microfluidic device for beamtime application. Figure 3.4 shows the pore plugging capability of AZAG within a PDMS microfluidic device, viewed under optical microscopy.

Figure 3.4: Aluminium salts forming gel plugs within PDMS devices, viewed with optical microscopy by BGG in preparation work for the microfluidic SAXS experiments carried out within this thesis. For scale, the vertical channel has a width of 300 µm

Chapter 4

Eutectic Solvents

1 Defining a Deep Eutectic Solvent

Eutectic solvents (ES) are a relatively modern form of solvents, first mentioned in 2003 by Abbott,[52] despite eutectic interactions or 'eutexia' being described as long ago as 1884 by Guthrie.[53] The popularity of purely eutectic solvents developed from the work of ionic liquids as solvents with 'environmentally friendly' properties, when it was discovered that a choline chloride : urea mixture featured a large depression in its melting temperature (24 °C) compared to the constituents (302 °C and 133 °C respectively).[54, 55] ESs have many favourable properties such as low volatility, low flammability and are considered environmentally friendly. Due to their properties depending on the compounds of which they comprise, they are 'tunable' and are considered to be designer solvents.

From first glance, ionic liquids and ES may appear to be similar, they both form a liquid phase when two compounds are combined at room temperature. This is both a good point of comparison but also where the similarities end.[54] An ionic liquid is just that, a chemical compound comprised of molten ionic salts at room temperature. Whereas a ES is a simple mixture of non-ionised chemicals which, in theory, could be separated back into pure compound A and compound B (in a two-component system).[56]

A eutectic mixture comprises of two or more compounds, which when combined in a mixture, cause a depression in the melting point from either of the independent compounds, due to favourable thermodynamic hydrogen bond interactions.[57] This eutectic phenomenon is commonly put into practice when gritting roads in cold weather, where the freezing point of water is lowered to

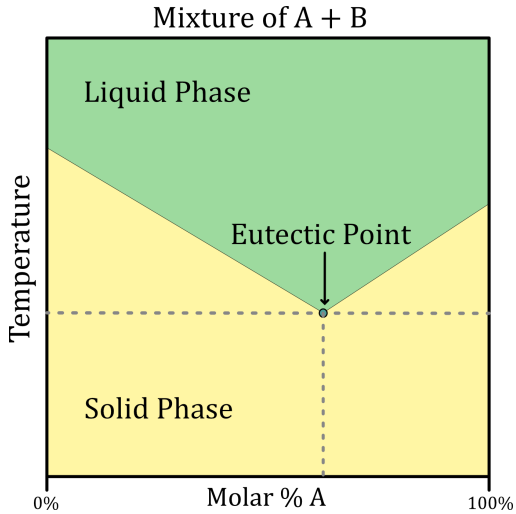

Figure 4.1: Phase Diagram of Mixture A and B which feature a eutectic depression.

prevent ice formation and is observed to some degree with all immiscible solids. In terms of eutectic solvents, this melting point should be at highest room temperature (25 °C), for the mixture to function practically as a solvent. The mixing of these components must not chemically change the chemical nature of the compounds themselves. In the case where a chemical reaction occurs between the solvent components, an ionic liquid can be formed or esterification can take place, forming another compound within itself.[58]

The definition of a deep eutectic solvent (DES) only extends this complexity and has been the topic of much debate since the first introduction of DES in 2003.[52, 59] The "deep" descriptor, perhaps used a little eagerly in some of the early publications of eutectic solvents, is now restricted to eutectic mixtures which feature a significant deviation from thermodynamic ideality of the melting point depression of the eutectic mixture.[57] Despite ever increasing specificity to which DES are defined, the magnitude of this depression has not been defined accurately in the literature. Therefore, the term 'DES' is used to describe the dodecanoic acid : menthol mixture in Paper II. However, the term 'ES' is used as a general term to describe the mixtures in Paper III, as not all of these solvents are qualified to carry the 'deep' descriptor.

DES are generally considered 'green' solvents due their production and use being in line with several of the principles of green chemistry.[60] They are produced by default with 100 % atom economy, and their purity is defined by the purity of their components, they seldom require heating or energy intensive 'synthesis' for their formation and many can be produced from entirely naturally occurring

compounds.[61] Despite this, it should be noted that although DES components can be produced through the extraction of natural products,[62] these compounds are quite often produced via or as by-products of industrial processes. These industrial processes are normally capable of producing higher chemical purity compounds at lower cost or without extensive purification steps, meaning that any environmental advantages of their use may be lost entirely if these solvents were to be used on an industrial scale. A classic case of this is the use of choline chloride which despite being naturally occurring and biodegradable, is generally produced via an industrial process and faces much restriction in its use, as it is a quaternary ammonium salt.[63]

2 Types of DES

Currently, DES are characterised into five separate groups, which are defined by the chemical properties of the compounds of which they consist, these groups can be seen in Table 4.1. Due to similarities between the compounds which make up the different groups, DES within the groups tend to have similar chemical properties, which allows the solvent to be tuned to a specific application.[56] The early DES (Type I) are formed from molten mixtures of quaternary ammonium salts and metal salts, with the next generation (Type II) utilising metal hydrates instead of the salts themselves. Type III DES still consist of quaternary ammonium salts such as choline chloride, but with the replacement of the metal salts/hydrates with a hydrogen bond donor such as glycerol, urea or an alcohol. Type IV DES use metal salts as in the earlier DES, but in combination with a hydrogen bond donor, similarly to Type III. Type V DES comprise of non-ionic hydrogen bond donors and acceptors.[64] These are especially useful as the components tends to be non-toxic and skin-safe, due to comprising of compounds such as carboxylic acids, alcohols and terpene molecules, allowing them to be rapidly biodegradable and sustainable, where produced from natural resources. This allows a significant advantage over the use of petrochemical-derived solvents which are not biodegradable, allowing their potential as replacements to these traditional solvents.

Table 4.1: The five types of Eutectic Solvents and their components

ES Type	Description
I	Quaternary ammonium salts / Metal salts
II	Quaternary ammonium salts / metal salt hydrates
III	Quaternary ammonium salts / Hydrogen bond donor
IV	Metal salts / Hydrogen bond donor
V	Non-ionic hydrogen bond donor / Non-ionic hydrogen bond acceptor

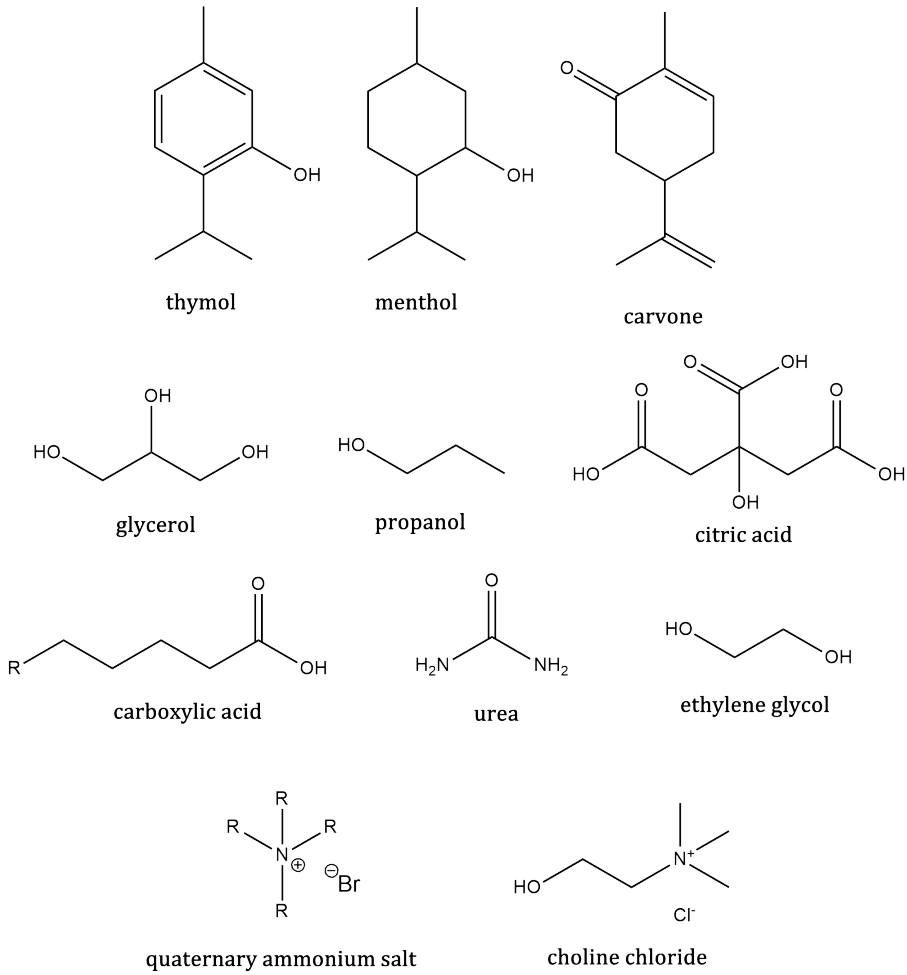

Figure 4.2: Some examples of molecular components for the five types of DES

3 Type V DES Properties

DES types I-IV tend to be limited in some applications due to their hygroscopic nature,[65] which cause them to significantly change their physicochemical properties through exposure to the atmosphere. They are also often limited due to their high viscosities,[66] which limit their practical usage. However, Type V DES have the advantage that they tend to comprise of hydrophobic chemic-

als such as fatty acids and terpenes and are hydrophobic themselves.[67] This characteristic allows the use of these DES to act similarly in applications to petrochemical-based oils such as mineral oil. Due to their hydrophobic nature, these DES phases can be suspended within a continuous aqueous phase, allowing the solubilisation of hydrophobic molecules to be delivered within an aqueous system. This type of emulsion is familiarly seen in products such as in milks,[68] paints[69] and personal care lotions.[70] Type V DES tend to be of much lower viscosity compared to the other DES types, which allows for greater scope of potential application as solvent extractants or currently used oil replacements.[71]

As the DES is comprised of hydrogen bonding moieties, this causes the formation of a macroscopically non-polar solvent with a network of nanoscale polar regions around the clusters of constituent hydrogen bond donor and acceptor groups. These nanoscopic regions arise due to the complex structures formed within the DES which allows the DES to interact and solubilise many compounds which are not soluble within their petrochemical analogues.[72–77] It is these highly tunable and varied properties which allow these mixtures to function in such varied environments, from battery electrolytes, to pharmaceutical applications.[78] They have also been used as extractants,[79] in gas capture,[80] electrolytes[81] and as replacement solvents in organic synthesis.[56, 79]

In the case of Type V DES, these solvents share many physicochemical characteristics with petrochemical oils. Also, like ionic liquids (ILs), they have increased solubilisation potential compared to mineral oils and therefore can stabilise a greater range compounds into their structures, whilst being simpler, cheaper and more environmentally benign to produce than ILs.[81] These similar solvents have been studied in greater detail with regard to ILs, where wide angle X-ray scattering peaks can be observed to elucidate the finest level structure between the solvent moieties, and these defined by their various types of interaction.[82] As many Type V DES components tend to be secondary metabolites of plants, such as menthol (from mint) and thymol (from thyme), they can be feasibly produced in large quantities through simple extraction from their parent plant, allowing them to be truly green, sustainable and biodegradable solvents.[83]

4 Benefits and Applications of DES

Ever since DES were first introduced for their potential applications as replacements for ILs as battery electrolytes, their applications have blossomed into many other fields as their favourable properties have been taken advantage

of.[54] This has allowed their use as alternatives not only to ILs, but also many industrially produced traditional solvents, which are normally derived from petrochemical sources. Due to the much lower viscosity of Type V DES and their hydrophobic makeup, they lend themselves to replace oily solvents such as mineral oil. This allows them to form emulsions with an aqueous phase and further extends their capabilities.[84–86]

Due to their fascinating characteristics, hydrophobic DES have been heavily investigated since their first publication, little over a decade ago by van Osch et al.[87] Their main purpose has been as extractants for a variety of compounds including fatty acids,[87] lipids, heavy metals[88] and aromatic hydrocarbons from aqueous media.[89, 90] Due to their low viscosity, they have also successfully been used to replace petrochemical based solvents (hexane) in synthesis reactions, where they improved the fatty acid conversion in an ester synthesis.

As many DES are produced from non-toxic and skin-safe molecules, they are suitable to deliver cosmetic and pharmaceutical molecules to the skin. This has lead to their use as skin permeation enhancers that deliver drug molecules more effectively.[83, 91] The antibacterial properties of essential oils such as menthol and thymol are also naturally antibacterial,[92] making them useful candidates to prevent infections occurring when used in wound dressings.[93]

Whilst not characterised as a DES, the eutectic effect was used for transdermal drug delivery for the first time in 1997.[94] The combination of combining menthol with the drug testosterone was found to greatly reduce the melting point of testosterone by over 100 °C, which dramatically increased its uptake through the skin. This greater uptake of drug molecules allows for faster acting medicines, potentially at reduced dosages due to greater therapeutic effect. This was also explored with ibuprofen in 1998, where various terpenes including menthol were combined with the drug for comparison of their trans-dermal uptake. It was found that terpenes capable of hydrogen bonding, and therefore a greater eutectic depression, cause greater uptake through the skin.[95]

Chapter 5

Emulsions

Emulsions have intriguing structures as they exist as a combination of two immiscible phases, with a microscopic assembly of the dispersed droplets within continuous phase which surrounds them. Emulsions can be either oil droplets in water (O/W) or water droplets in oil (W/O). This unstable situation is achieved when energy is supplied to the system, dividing the dispersed phase into droplets as seen in Figure 5.1. The formation of an emulsion allows the continuous phase to act as a carrier of the dispersed phase, where there are many applications from foodstuffs to industrial paints.

Emulsions, such as milks, are abundant in nature. In the laboratory there are many methods of producing them synthetically, such as high shear mixing[96], membrane emulsification,[97] or as was used in Paper II, ultrasonic emulsification.[98] Although this method has limitations when upscaling to industrial quantities, it was suitable for lab scale production as the conditions are easily controlled and therefore replicated between different laboratories, which was necessary for preparing samples at a research facility. The equipment used is cheap and suitable for sample sizes as small as 0.5 mL, which became useful when producing samples comprising expensive deuterated chemicals for neutron scattering experiments.

1 Emulsion Stabilisation

When the two phases are emulsified, the dispersed droplet phase has much greater exposed surface area to the continuous phase, forming an energetically unfavourable state. As the dispersed phase droplets collide with one another

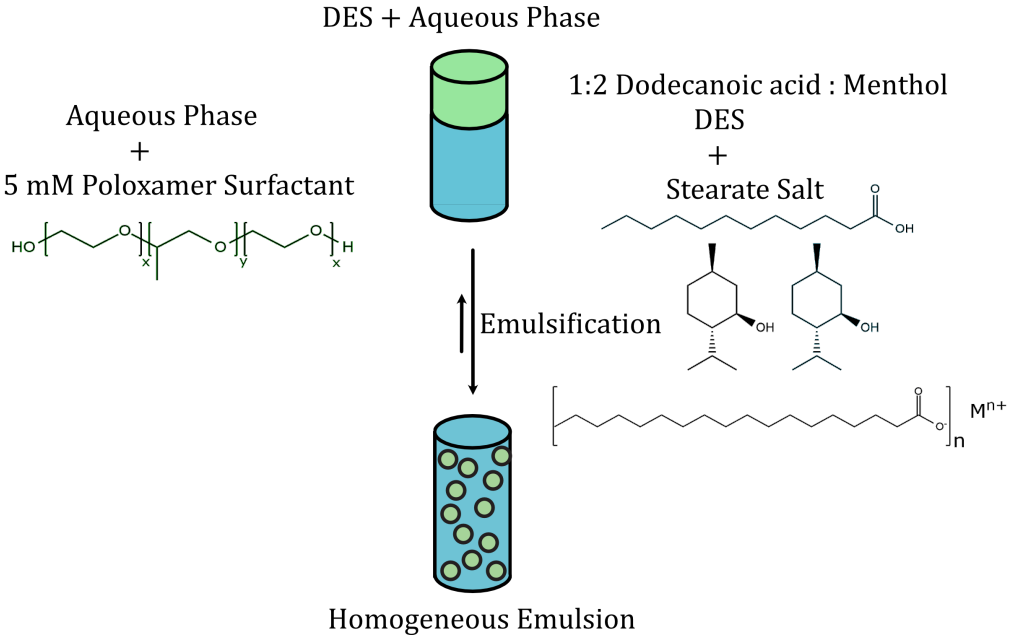

Figure 5.1: An illustration of the components in a DES emulsion, as studied in Paper I

within the continuous phase, they will coalescence, to a lower energy state as the exposed droplet surface area is reduced. This effect causes the droplets to form increasingly larger droplets through the Ostwald ripening, [99] which is illustrated in Figure 5.2. Without stabilisation, the emulsions will rapidly break down into their constituent phases, forming two bulk phases once more.

There are several ways to stabilise emulsion droplets, which mainly involve modifying the emulsion surface to prevent droplet coalescence. Pickering emulsions are stabilised by dispersions of small solid particles upon the droplet surface, forming a physical barrier between colliding droplets.[100–102] This method was used by Bryant et al. who stabilised DES emulsions with oxidised cellulose nanofibrils, which were stable to a minimum of 200 days.[84] Charged surfactants such as sodium dodecyl sulphate (SDS) stabilise the emulsion surfaces through electrostatic repulsions, as investigated in DES emulsions by van Osch.[99] Viscosity modifiers can also be used to thicken the continuous phase to entrap the stationary phase droplets within, immobilising them and preventing their coalescence. Moreover, non-ionic surfactants such as Tween20 have been used by Syed to stabilise nanoemulsions produced via membrane emulsification.[85, 86] These non-ionic surfactants stabilise the emulsion surface through steric interactions, where the hydrophilic surfactant head groups anchor in the aqueous phase, and the hydrophobic tails stabilise in the oil phase, preventing droplet coalescence.

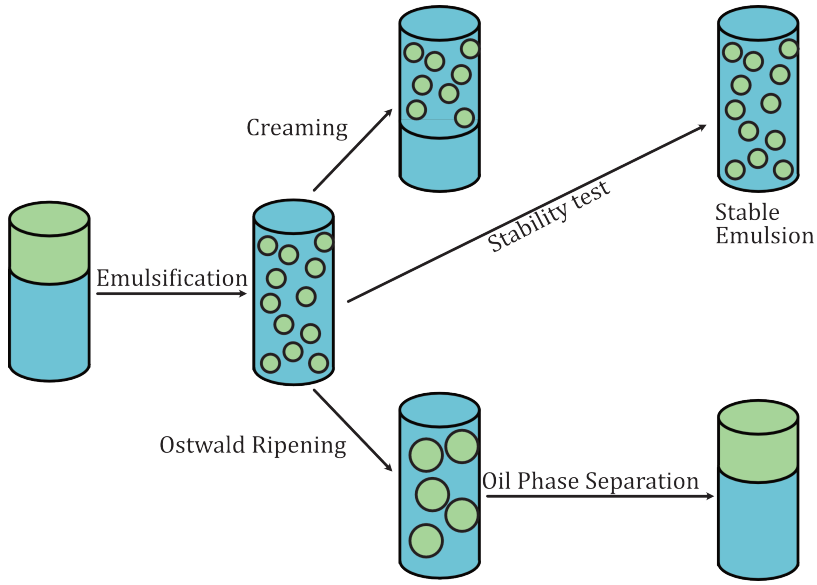

Figure 5.2: An illustration showing the various ways an emulsion can become unstable

Within Paper II in this thesis, non-ionic surfactants were used in the stabilisation of DES emulsions, where it was found that stearate salts altered the nature of the surfactants, further improving the emulsion stability. In Chapter 6, surfactant self assembly and packing is introduced, to provide context for Paper II.

Chapter 6

Surfactant Self Assembly

Surfactants are, by definition, surface active chemicals. This is due to their amphiphilic properties which arise from their hydrophilic 'heads' and hydrophobic hydrocarbon 'tails'. This causes these molecules to self-assemble, to minimise unfavourable energetic interactions. The nature of this mechanism depends on many environmental conditions such as temperature, solvent polarity and the presence of contaminants in the solution such as ions. The surfactant structure of course plays a large part in its characteristics where its concentration and composition affects properties of the surfactant in solution such as it's critical packing parameter (CPP) and critical micelle concentration (CMC). These parameters are used to define the properties of surfactants which allow them to be classified for use in industrial products/processes.

Surfactants are present in the bulk solution as free molecules at low concentration, where they aggregate at the surfaces to reduce unfavourable interactions of water molecules with the hydrophobic regions. As the surfactant concentration increases, the likelihood of forming micelles also increases, due to favourable entropic interactions. Although, the specific concentration that this occurs, known as the critical micelle concentration (CMC) is dependant on a range of factors, including the surfactant in question itself. At the CMC, these micelles are more energetically favourable due to the limited interactions between the hydrophobic tails with the hydrophilic solvent, as the micelles aggregate to maximise the solvent interactions with the head groups and minimise the solvent interactions with the tails. As the surfactant concentration increases past the CMC, the free surfactant concentration remains constant, where additional surfactant molecules aggregate to form micelles.

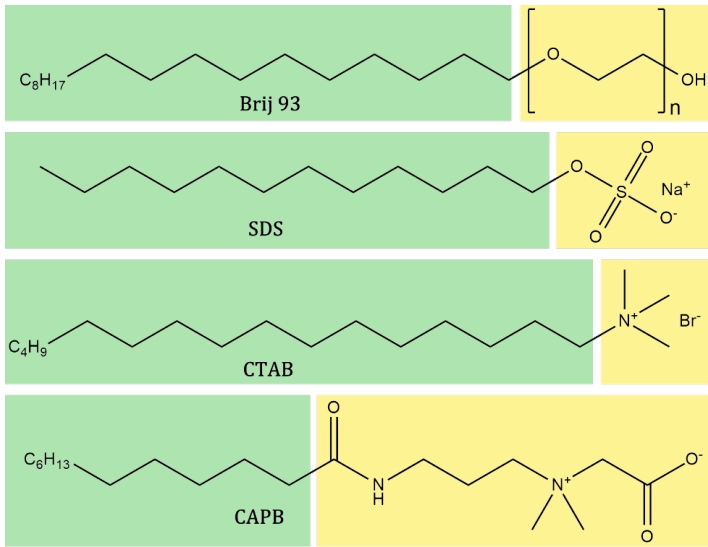

Figure 6.1: An illustration of a typical surfactant molecules, showing the hydrophilic head (highlighted in yellow) and hydrophobic tail (highlighted in green).

1 Critical Packing Parameter

The critical packing parameter of a surfactant is a prediction of the geometry of a surfactant in solution, and depends on the relative sizes of the hydrophilic head groups to hydrophobic tail groups within the molecule. This can be calculated according to Equation 6.1, where p = critical packing parameter, v = volume of hydrophobic tail, l = length of the hydrophobic tail and a_o = optimal head group area.[103]

$$p = \frac{v}{l.a_o} \tag{6.1}$$

Table 6.1: The critical packing parameters and their respective surfactant phases which form due to the self assembled geometries.

CPP	Surfactant Phase
0 <1/3	Spherical micelles
1/3 <1/2	Wormlike micelles
1/2 <1	Vesicles or flexible bilayer membrane
1	Planar Bilayer (Lamellar)
>1	Inverted micelles

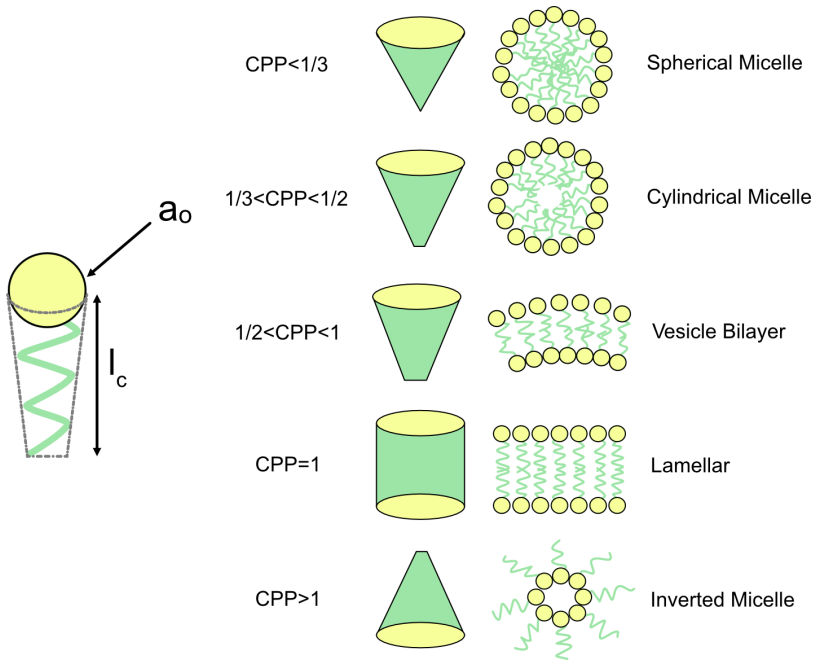

Figure 6.2: The surfactant phases of a range of critical packing parameters, recreated from [103]

Although these packing parameters predict the surfactant structure, they are not a definition of the structures formed, with many variables factoring in to the true self assembled nature. Temperature is a key factor in this, causing surfactants to undergo phase transitions between many of the phases in Table 6.1, depending on the environmental conditions. The transitions between these phases allow for interesting features of materials engineering, allowing samples to act/change their chemophysical properties. Gelation triggers can often be characterised for example by the transition of amphiphilic compounds from a solution (micellar) phase to gel (lamellar) phase.

2 Poloxamer Surfactants

Poloxamer (also known as Pluronic) surfactants are synthetically derived, non-ionic triblock copolymer surfactants consisting of (poly) ethylene oxide (PEO) and (poly) propylene oxide (PPO) subunits with a (PEO-PPO-PEO) general formula. By altering the stoichiometries of x and y in the general structure of $EO_xPO_yEO_x$ (see Figure 6.3), the hydrophilic-lipophilic balance (HLB) can be altered, as shown in Table 6.2. This is due to the relative hydrophilicity of the PEO groups and the hydrophobicity of the PPO groups respectively. As the quantity PEO and PPO blocks increase in the surfactant, the amount of stabilisation in each of the oil and water phases respectively increases. This tailorability of the surfactant allows for much choice of which poloxamer surfactant to use for a specific purpose, such as when stabilising oil : water emulsion interfaces, as is discussed in Paper II. These surfactants are also non-toxic which enable them to be used in a myriad of applications including food, personal care and pharmaceuticals. [104] Depending on their composition, concentration and temperature, these polymer surfactants form different aggregated phases including micelles and lamellae, where the ratio of PEO to PPO subunits controls which surfactant phase is formed. [105–109] At higher concentrations, they form thermoresponsive gels which allow them to release drugs at a controlled rate into the body. [110–112]

Table 6.2: Poloxamer surfactants used in Paper II and their properties

Name	Formula	MW (g mol^{-1})	HLB
Poloxamer 182	$(EO)_{04}(PO)_{30}(EO)_{04}$	2050	1-7
Poloxamer 184	$(EO)_{10}(PO)_{30}(EO)_{10}$	2650	10-12
Poloxamer 334	$(EO)_{20}(PO)_{60}(EO)_{20}$	5700	10-12
Poloxamer 407	$(EO)_{90}(PO)_{60}(EO)_{90}$	12600	>24

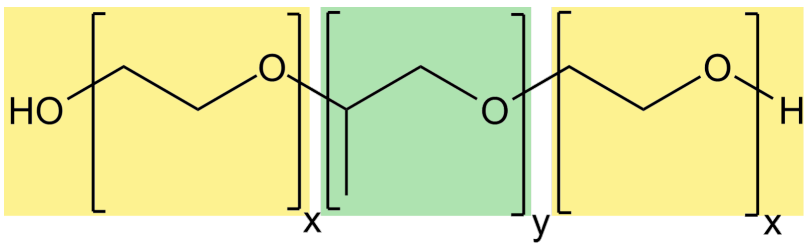

Figure 6.3: The general composition of a poloxamer surfactant

The self-assembled structures of poloxamer surfactants at the interface of a hydrophobic DES emulsion is the topic of discussion in Paper II, where we

discuss the packing of the surfactant structures and how this changes on the addition of stearate salts.

Chapter 7

Gelation

Gelation refers to the liquid-solid phase change in a material otherwise known as a sol-gel transition. During this transition, the gelator molecules form a network within the solvent, entrapping it within. The amount of gelator in a sample can be less than 1%, but still are able to cause the whole sample to form a gel. This occurs on application of a 'trigger', which could be a change in temperature,[107] solvent environment,[113] pH,[114] application of shear or the addition of a salt.[115–117] Some of these gelation triggers are reversible and some permanent, depending on the nature of the gelator and hence the bonds formed within the gel network.[118, 119]

As gel phases exhibit properties of both liquids and solids, they are able to hold their own shape like solids but can also deform like liquids. This allows them to be useful to soft matter chemists as these materials stand on the boundary between these two phases. This allows the gels to gradually release drug molecules, such as within medical bandages loaded with hydrogels,[120] or form gels to entrap pollutant molecules.[121]

Gels are either permanent or reversible, with the former normally forming much stronger gels featuring covalently cross-linked polymers and the latter normally formed from non-covalent linkages between gelator molecules. These non-covalently bonded gels are comprised of branched and/or entangled networks of self-assembled fibres of gelator molecules. These networks are usually weaker and reversible, so break and reform as temperature or pH varies due to external stimuli. Gels can also be formed through coordination of ionic species to charged residues, which causes non-covalent cross links to be formed between gelator molecules, immobilising the solvent within.[122]

The physicochemical properties of surfactant self-assembly and gelation are closely linked. As described in Paper II, the formation of a gel can sometimes originate from a compact surfactant phase, where the same molecules form surfactant aggregates and gels under different conditions if above the critical gelation concentration.[113] This effect is seen with thermoreversible gels of poloxamer surfactants.[104, 108]

1 Low Molecular Weight Gelators

Gels formed via low molecular weight gelators (LMWG) such as hydro-, organo- or eutectogels[123] (formed in aqueous, organic or eutectic solvents respectively) are self assembled, fibrous and normally reversible gels that can be triggered under specific conditions. [118, 124] These tend to be formed from entangled fibres of the LMWG, forming fairly brittle and stiff gels. This causes them to be fairly inflexible but have been proven to be useful for certain applications, such as gradual release or capture of compounds from a gel networks,[125, 126] chemical sensors[127] and for optoelectronic devices.[128]

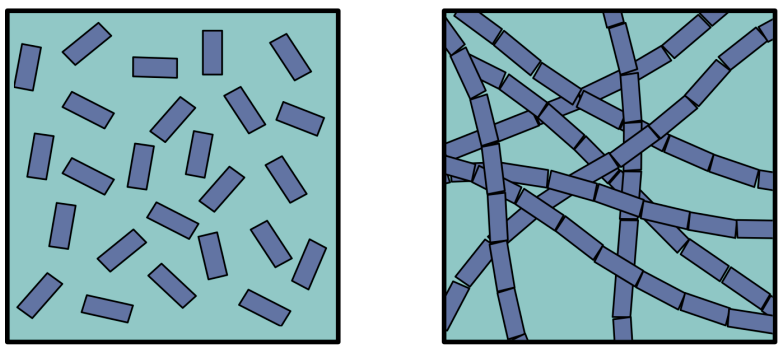

Figure 7.1: An illustration of a solution (light blue) containing gelator monomers (dark blue), which are present below the critical gelation concentration (CGC) and a 3D network of hydrogen bonded gelator molecules, immobilising the solvent.

2 Solvent Effects on Gelation

The properties of a gel are dependent on a range of factors. The gelator itself and the bonds formed between the molecules to form the network plays a large part, but the environmental conditions can also greatly affect the gel structure.

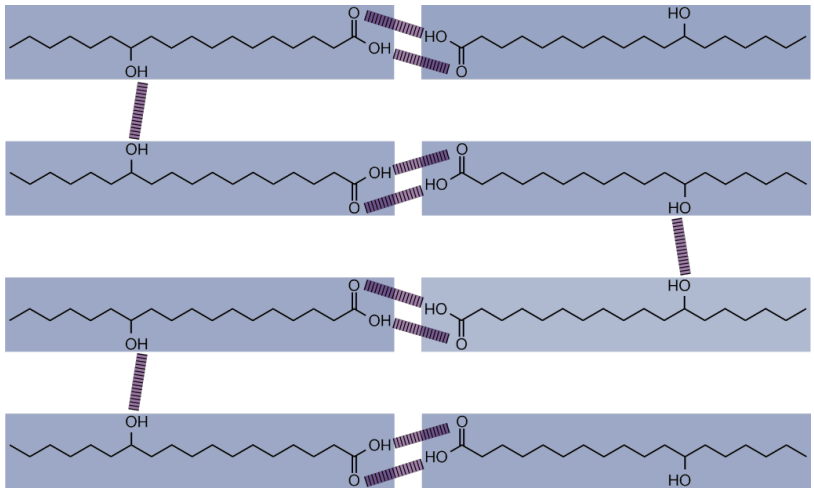

Figure 7.2: An illustration of the self-assembled HSA gel network formed of hydrogen bonds (purple) between dimerised pairs of HSA molecules (blue), which extends throughout the solvent, entrapping it within. Recreated from Roddy et al. (2025), with permission under CC-BY license.[129]

The solvent environment has a large effect on the gel strength. This can cause gelator molecules to disperse, weakening the gel structure, or aggregate, strengthening it. This can be seen in the kitchen, when one prepares an edible jelly. The solvent (normally water) allows a gel of desired strength to be formed. However, if the solvent is modified, such as if ethanol is added when making 'jelly shots', it is less likely to form a gel, due to the unfavourable solvent modification.

This is shown in the literature with HSA-based organogels, where the varying solvent polarity formed gels of varying strength.[130] The solvent structure could also be modified by addition of hydrogen bonding additives, which affect the gel structure by preventing fibre formation or by bridging gelator molecules. This gelator is the focus of Paper III within this thesis, where instead of organic solvents, ES have been used. The HBA and HBD molecules which form the ES were varied and stoichiometries altered to explore the effect of the solvent environment on the gels formed within them.

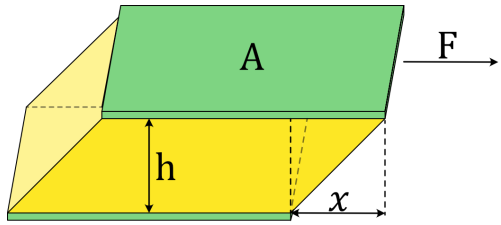

Figure 7.3: A schematic showing the measured dimensions during a rheological measurement. Area (A) of the surface in contact with the sample applying the force (F) during shear experiments on a sample with a thickness/height (h) where the sample is sheared by distance (x) due to applied strain (γ).

3 Rheology

Rheology is the study of flow and deformation of materials. This can be applied to both fluids and viscoelastic solids which exhibit both liquid and solid-like properties. The simplest of rheological measurements could involve observing the difference in flow rate of a viscous liquid such as honey gradually creeping down the side of an upturned jar and comparing the speed at which this occurs when the honey is heated above room temperature. More technical experiments involve the use of a rheometer, which can simultaneously measure many variables that are applied to a sample, or measured in response to stimuli such as shear, stress or change in temperature.[131, 132]

3.1 Viscoelasticity

Viscosity is a measure of how much energy is required to deform a fluid, which can be affected by temperature, pressure and shear. Generally, increasing the temperature of a fluid will decrease its viscosity, such as when warming syrup to allow easy dispensing. Shear flow is observed when a 'layer' of fluid passes over another and measures the ease at which this occurs. In rheology experiments the bottom layer is stationary whilst a force F acts upon the top layer of unit area A allowing the stress (σ) to be calculated, as in Equation 7.1. This applied stress causes the top layer to 'shear' a distance x, meaning that the top layer is now displaced laterally from the bottom layer. The distance x divided by the total height of the sample h is termed the shear strain (γ), see Equation 7.2. For solid samples, no flow is possible and therefore the strain will reach a maximum value as stress increases.

$$\sigma = \frac{F}{A} \tag{7.1}$$

$$\gamma = \frac{x}{h} \tag{7.2}$$

$$strain\ rate = \frac{d\gamma}{dt} \tag{7.3}$$

As the shear stress applied to the top layer of the sample is transferred through the layers of the sample by the 'layers' of the sample interacting with one another, the effect of the force placed on the top layer is dampened, reducing the fluid velocity. As the shear strain varies with shear stress, the coefficient of proportionality between the values is termed the dynamic viscosity η.

$$\gamma\eta = \sigma \tag{7.4}$$

3.2 Storage & Loss Modulus of Viscoelastic Materials

The key parameters recorded from rheological experiments are storage (G') and loss modulus (G") (also referred to as elastic and viscous moduli respectively, viscosity and yield stress). Storage modulus is a measure of how much energy is stored in the sample when stress is applied. As the sample deforms, the energy is stored in materials with a high storage modulus (those which are more solid-like). Loss modulus measures the amount of energy dissipated within the sample due to deformation of the sample itself, while viscous samples will require a lot of energy to shear, this energy isn't stored like in an elastic sample. Both of these moduli are important to identify the nature of a material and its state is defined due to the relative magnitudes of its storage and loss moduli. If the storage modulus is higher, the material is a solid. If the loss modulus is higher, it is a liquid sample. $\tan\delta$, calculated by dividing the loss modulus by the storage modulus, which can be compared to define the viscoelastic properties of a material. By measuring the storage and loss moduli with time or temperature, gelation processes can be monitored and samples can be compared, as in paper III in this thesis.

3.3 Oscillatory Measurements

If the material is purely elastic, the applied stress is directly related to the strain observed with the constant of the storage/elastic modulus (G) and can be calculated as in Equation 7.5.

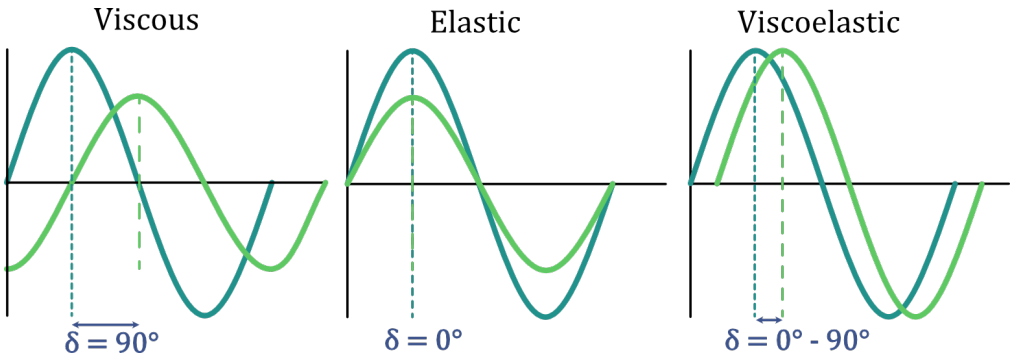

Figure 7.4: An illustration of the viscoelastic properties of a gel. The Blue lines represent the applied stress and the green lines represent the measured strain. The δ value is a measure of phase delay

$$\gamma = \frac{\sigma}{G} \tag{7.5}$$

If the material is purely viscous, the applied strain is permanent as there is no energy stored within the fluid. The amount of stress can be calculated in Equation 7.6.

$$\gamma = \frac{\sigma t}{\eta} \tag{7.6}$$

Oscillatory measurements allow the stress and strain to be calculated from known sample height (h) and applied torque and oscillatory frequency. Either stress or strain amplitude must be also controlled to calculate the other. Where stress is controlled, the angular displacement is measured, from which the strain can be calculated. If the strain is controlled, the angular displacement is controlled and the amount of torque required from the rheometer is recorded, to calculate the required shear stress. This gives the complex modulus (G^*) which allows the materials resistance to deformation to be calculated, as in Equation 7.7.

$$G^* = \frac{\sigma_{max}}{\gamma_{max}} \tag{7.7}$$

By plotting the maximum stress against the maximum strain, the relationship between these can be observed. If the material is purely elastic, there will be 0° phase difference between the maximum stress and the maximum strain. Where the sample the material is purely viscous, there will be a 90 ° phase delay. The

phase difference can be quantified by δ, which quantifies the amount of the elastic and viscous contributions, giving the storage and loss moduli.

$$G' = G^* cos\delta \tag{7.8}$$

$$G'' = G^* sin\delta \tag{7.9}$$

$$tan\delta = \frac{G''}{G'} \tag{7.10}$$

3.4 Linear Viscoelastic Region

The linear viscoelastic region (LVER) is a region of rheological space that defines the point at which the material degrades as its limit. Within the LVER, as the stress (or strain) on the sample is gradually increased, the storage modulus of the material remains constant up to the limit. Beyond this limit, the microstructure breaks down as the sample yields, causing a non-linear relationship between stress/strain and the storage modulus from this point. This occurs at different shear strains for different materials and is an important consideration when conducting rheology measurements, to ensure that the material is not being degraded during measurement. To find this, a simple oscillatory stress (or strain) sweep can be performed on the material, which shows where the material begins to break down, as illustrated in Figure 7.5. Determination of the storage and loss moduli of the eutectogels studied in this thesis were conducted within this region.

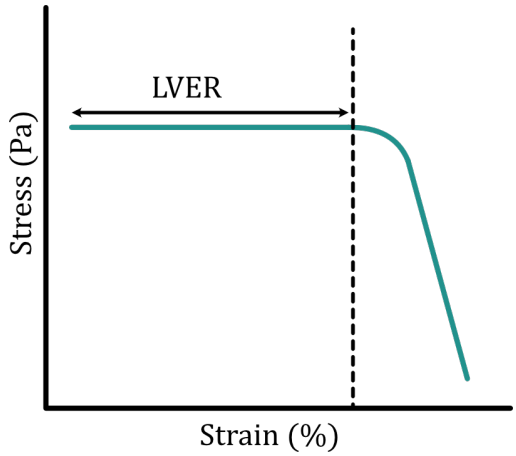

Figure 7.5: Graphical illustration of the determination of the LVER of a sample

Summary of Results

In relation to the aims of the thesis laid out in the Thesis Objectives, the results are summarised here.

In chronological order of the work completed, the work presented within this thesis firstly looks into the action of aluminium salts currently used as antiperspirants. This was achieved through the use of a custom designed and fabricated microfluidic device, with aims further improve the work completed by other research groups in the literature. This work is presented in Paper I.

After this period of study into microfluidic devices, the work focus moved towards potential novel carrier solutions for personal care actives. This culminated in the works presented in Paper II and Paper III, the first of which utilises a type V DES to form an emulsion dispersed phase, as a potential novel replacement to mineral oil based emulsions.

Paper III uses Type V eutectic solvent components in an array of 25 eutectic mixtures to form varying solvent environments. Within these solvents, the low molecular weight gelator was introduced to form eutectogels with varying gelation properties. The macroscopic properties of these gels are explored with rheological methods and the nanoscale structure is probed with SAXS to rationalise the observed macroscopic characteristics.

Paper I: A Microfluidic Study of the Eccrine Sweat Gland Environment with a High Transmission SAXS Device

Aluminium salts are used as antiperspirant actives in a range of products across the globe. As discussed in Chapter 2, these salts react with proteins naturally occurring in the eccrine sweat gland, forming gels which prevent sweat flow to the skin surface. This paper firstly discusses the design of a multi-layered microfluidic device, specifically for use on a synchrotron beamline. The aim of this project was to improve the SAXS data available when conducting *in situ* microfluidic experiments on a beamline.

The microfluidic device was designed in Fusion 360 (AutoDESK) software as seen in Figure 7.6, and the parts milled on a CNC milling machine (Daltron). This design, which is shown in Figure 7.6 included high pressure liquid chromatography (HPLC) style ports, enabling the attachment of HPLC style PEEK connections with PEEK tubing which allowed superior reliability of fluid connection compared to friction fitted or glued connections as employed in other microfluidic devices which are prone to air-ingress. This method also allowed a convenient way to attach and detach the tubing as required during experiments. A T-shaped section runs through all layers, barring the window material, with a filleted section to allow the beam to pass through without interference from the body of the device. Pins were positioned in the bottom plate to align the layers, with the appropriate holes in the layers throughout the device. Several window materials were tested for use in the including Kapton and Mylar, but cylic olefin copolymer (COC) was selected for synchrotron experiments due to the lack of scattering features in the SAXS region (q = 0.01 - 1 Å^{-1}, which allowed for easier visualisation of the scattering features arising from the solutions. The window material was 75 µm thick, and was separated by a 120 µm aluminium channel layer, which allowed for a high X-ray transmission device and good quality scattering data to be collected in 50 ms collection times. For ensuring that the device remained water-tight, 300 µm thick silicone gaskets were used between the layers, which were compressed together with 11 machine screws, with nuts and washers to firmly clamp the layers together. Furthermore, the multi-layered design allowed the device to be disassembled, the window material and gaskets replaced, without having to discard the entire device. As two identical microfluidic devices were machined, one could be used on the beamline whilst the other was cleaned and re-assembled during beamline experiments.

The device, due to its construction, had a high X-ray transmission. This allowed SAXS patterns to be collected in 50 ms exposure times and an array of 35 patterns could be collected approximately every 2 minutes, meaning that the scattering patterns could be compared over a period of time. whereby the

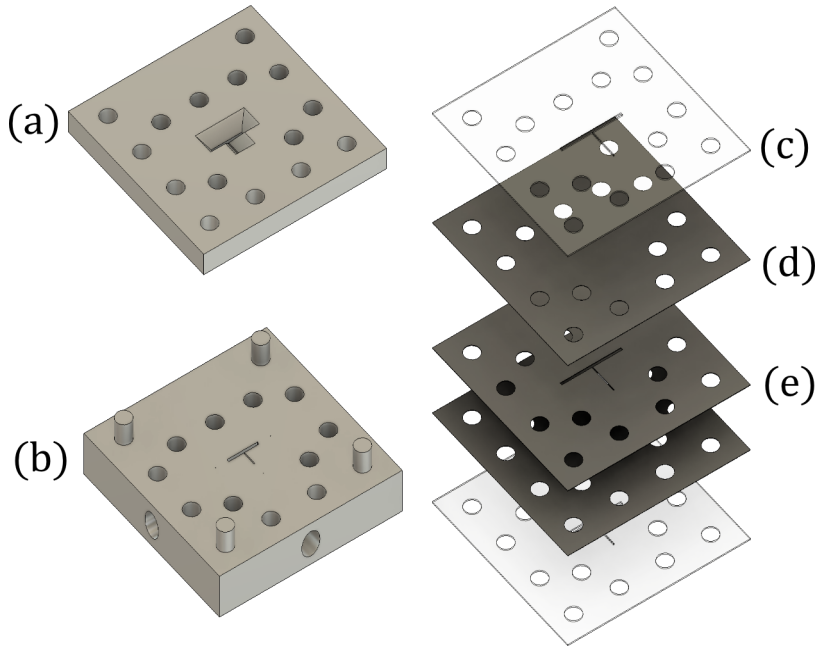

Figure 7.6: The multi-layered microfluidic device, shown in exploded view. The components which it comprises are as follows; (a) top plate, with filleted section to compress layers together for water-tightness, with filleted section to prevent impingement of X-ray beam; (b) bottom plate with milled fluidic ports within, HPLC ports for fluidic connection and alignment pins at each corner; (c) silicone gasket material, to seal the device; (d) COC window material; (e) The channel layer, which forms the channel dimensions, in this case the thickness was 120 µm.

developments in the structures present in the microfluidic channel could be recorded in a time-resolved manner.

Using transmission measurements, which were collected simultaneously to the SAXS patterns, a map of the area of the channel could be drawn, showing the positions where aluminium salt solution was present, due to its much higher SLD than other solutions (see Figure 7.7). This does form a good visual aid in understanding the flow of the two solutions and how they combine but was not sensitive enough to observe gel formation in the channel.

Despite difficulties during the beamline experiments, as the aluminium gel didn't adhere to the channel walls as in PDMS-glass microfluidics which further hampered by the vertical alignment of the microfluidic device, gel formation was observed in a few measurements. As shown in Figure 7.8, the gel structure is seen to change on combination with the artificial sweat within the microfluidic junction at various points within the channel during a single scan, showing the sensitivity of the SAXS measurements, even within these short exposure times.

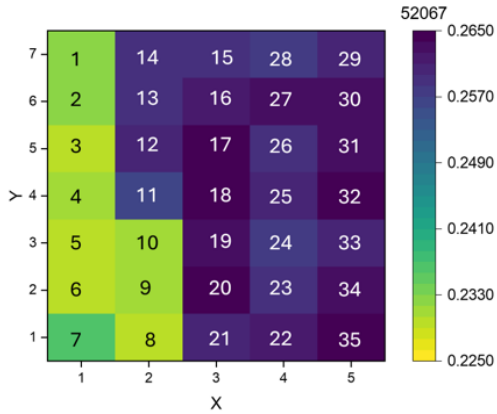

Figure 7.7: A transmission map of the microfluidic channel, showing an x,y plot of the channel intersection, with the colour shading representing the transmission value

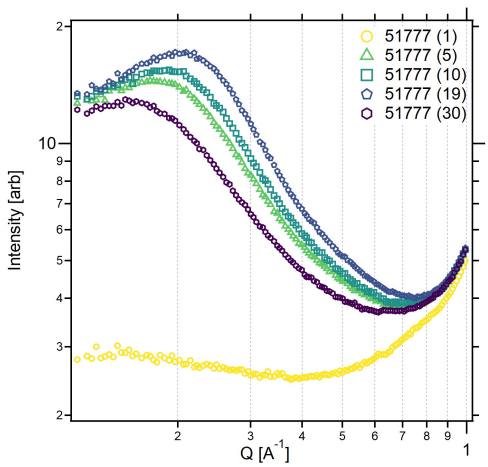

Figure 7.8: The SAXS patterns of a range of points in the microfluidic channel of scan 51777, when the sweat solution and aluminium salt solution are combined.

In conclusion, this work did make improvements on work found in the literature in some aspects, due to improvements of the SAXS range available. However, the surfaces of the aluminium channels did not provide a favourable surface to allow the adhesion of the aluminium salts, unlike in PDMS-glass based microfluidics. This prevented gels growing reproducibly within the microfluidic channels and therefore the action of the aluminium salts could not be compared with this device. However, the microfluidic device had a very high X-ray transmission, allowing high quality SAXS data to be collected in very short exposure times.

Paper II: Emulsions of Hydrophobic Deep Eutectic Solvents Stabilised with Poloxamer Surfactants and Stearate Salts

Dodecanoic acid and menthol are renewable and environmentally benign chemicals, which can be extracted simply on an industrial scale, making its large scale production and use feasible.[56] These chemicals are also biodegradable and therefore can be safely disposed of, once at the end of their usable lifetimes. The DES formed from combining these compounds, produces a liquid at room temperature with low vapour pressure and high thermal stability.[133] The DES is also hydrophobic, lending itself for a replacement for solvents and oil in a variety of applications including acting as the oil phase in an emulsion system.[84, 134]

This paper shows the work completed to stabilise emulsions formed from a hydrophobic DES with triblock copolymer (poloxamer) surfactants. Small angle neutron scattering (SANS) allowed these structures to be observed with greater clarity than SAXS, with the help of increased contrast available when using deuterated water (D_2O contrasting the hydrogen containing dispersed phase.

DES in water emulsions were formulated to explore if the stearate salts of sodium, calcium and magnesium would act as Pickering particles, to stabilise the emulsions. It was found that on addition of these salts to the formulations, the emulsion stability increased. However, no sharp crystalline peaks were observed in SAXS measurements of the bulk samples, giving no evidence to support that there were crystals stabilising the emulsion interface. As the emulsions were slightly more stable on addition of stearate salts, but not incredibly so, four poloxamer surfactants were added to the emulsion formulations to see if their stability could be improved further. It was found that the surfactant with the largest hydrophilic component (P407) improved the emulsion stability by the most, forming emulsions which were stable for over 1 month. More intriguingly, on combination with the stearate salt and poloxamer, the stability was further improved. The visual observations of the stability of the emulsion samples were confirmed using droplet size measurements, where the addition of stearate salt was seen to improve the polydispersity of the emulsion droplets, as shown in Figure 7.9. These findings lead to the application of SANS beamtime, to determine the increase in emulsion stability.

The SANS patterns, as seen in Figure 7.10, showed the presence of sharp, smooth interfaces of the emulsion droplets with a characteristic q^{-4} decay. However, where P407 was used to stabilise the emulsion, distinct scattering features were also present superimposed on this feature. For the emulsions stabilised by P407, the scattering features were fitted to a lamellar paracrystalline stacks model,

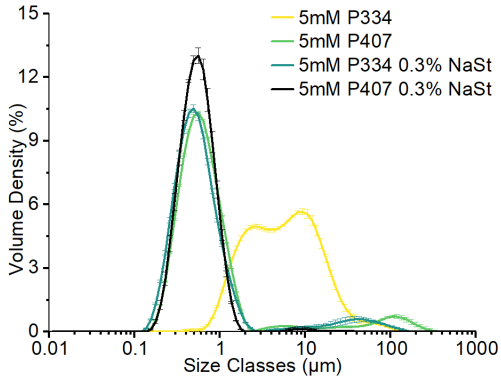

Figure 7.9: Droplet sizing data showing the effect of polydispersity on addition of NaSt to emulsions stabilised by P334 and P407 surfactants, measured after a 4 week storage stability test at room temperature.

which was justified through the comparison to literature precedents in similar systems studying emulsions and foams.

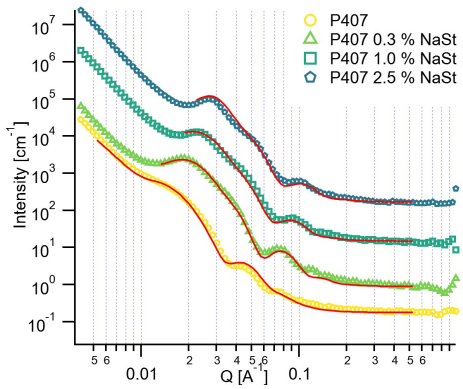

Figure 7.10: SANS patterns, collected on SANS2D, ISIS, UK. The scattering features are seen to shift to higher q with increasing NaSt concentration.

The fitting results illustrated the increase in density of the surfactant packing at the emulsion interface on addition of the NaSt. This was attributed to the kosmotropic effect of the salt on the hydrated polyethylene oxide (PEO) head groups of the poloxamer,[135, 136] which dehydrated them, increasing their packing density. This formed more robust interfacial structures which we proposed were akin to the poloxamer gels formed at higher surfactant concentrations under bulk conditions. These robust structures reduced droplet coalescence and therefore increased emulsion stability which explained the synergism between stearate salts and poloxamer surfactants.

Paper III: Gelation of 12-Hydroxystearic Acid in Type V Eutectic Solvents

Eutectic solvents (ES) comprise complex nanoscopic polar domains, similarly to ILs.[137] However, on a bulk scale, these yield non-polar characteristics. These nanoscopic domains arise from the alternating nature of polar sites where hydrogen bonding occurs between HBAs and HBDs with non polar moieties in the interstitial zones. This allows the different ES to feature varying chemophysical properties, depending on the HBAs and HBDs of which they are composed. The work in Paper III explores how, through the use of a range of HBA and HBD combinations, the solubility and therefore the gelation characteristics of a well known low molecular weight gelator (LMWG) 12-hydroxystearic acid (HSA) can be affected.

HSA has been previously studied in a plethora of solvents,[117, 129, 130, 138, 139] where generally the solvent polarity is the key factor in gel formation. This is because HSA forms fibres through intermolecular hydrogen bonds between other HSA molecules, which are disrupted by competition from solvent molecules. As the solvent polarity increases, the critical gelation concentration also increases. In non-polar solvents such as dodecane, there is little competition for the hydrogen bonding sites, strong gels are formed at low HSA concentrations; in more polar solvents such as alcohols, the HSA hydrogen bonding is disrupted, leading to higher required gelator concentration to form a gel.[130]

33 binary eutectic mixtures of hexanoic acid, octanoic acid, decanoic acid, dodecanoic acid, menthol, thymol and camphor were combined in various stoichiometric ratios, with stirring and heating to 50 °C to form liquids at room temperature. These mixtures were then stored under ambient laboratory conditions for a week, to ensure their stability as ES, any samples which crystallised during this period were discarded from further studies. From this stage, 25 mixtures remained as homogeneous liquids at room temperature, and were subjected to further testing.

These solvents were used to dissolve the HSA at 60 °C at concentrations between 1-20 wt.%. After dissolution at this elevated temperature, the mixtures were cooled back to room temperature and observed after 24 hours, where their physical states were assessed by visual observation and inverted, to assess whether the sample had formed a gel. It was discovered that the different ES combinations induced varying gelation properties on the HSA, where the different solvents formed gels at different concentrations. In order to assess the varying gelation properties in a quantitive method, the gels were subjected to frequency sweeps using an Anton Paar rheometer. It was found that the combination of

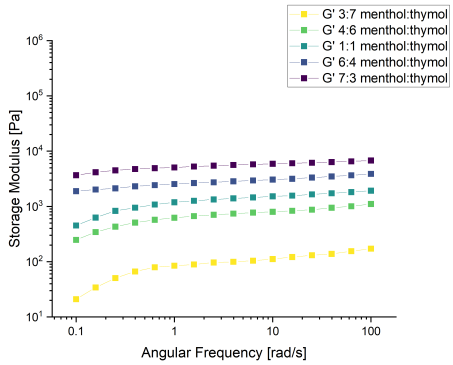

Figure 7.11: The rheological frequency sweep results, showing the varying storage modulus with increasing menthol molar ratio in a menthol : thymol ES.

the HBA and HBD and also the relative stoichiometry between these components caused significant differences in the strength of the formed gels, as seen in Figure 7.11.

In order to assess the gel structure within the samples, they were subjected to polarised optical microscopy (POM) and SAXS measurements. These analyses showed that the nanoscale fibre structure of the HSA largely remained the same within the solvents, but the different solvents promoted or limited the density of the fibre structure forming, as seen in Figure 7.12.

As HSA was seen to form gels of varying strengths, depending on the solvent environment, this was attributed to the nature of the hydrogen bonding between the HBA and HBD. Therefore, we discuss the interplay between the hydrogen bonding between the ES sites and the OH group on the dimerised HSA molecules, which was not a simple relationship. For example, stronger gels were generally formed in ES containing camphor, whilst the weakest formed in ES containing thymol. However, in camphor : thymol ES, the strongest gels formed out of all tested combinations. This was ascribed to the relationship between the relationship between the ES molecules preferentially forming hydrogen bonds between one another, which is shown by their very significant eutectic depression when the ES components are combined to form the solvent(-95 K, according to COSMO-RS predictions).[140, 141] The preferential bonding between solvent components leaves HSA to form fibres unimpeded the solvent, forming dense networks.

The SAXS patterns were used to gain understanding of the nature of the fibre structure. Where no gel phase was formed, the gelator molecules remained amorphously arranged in the solvent, without any significant structures ob-

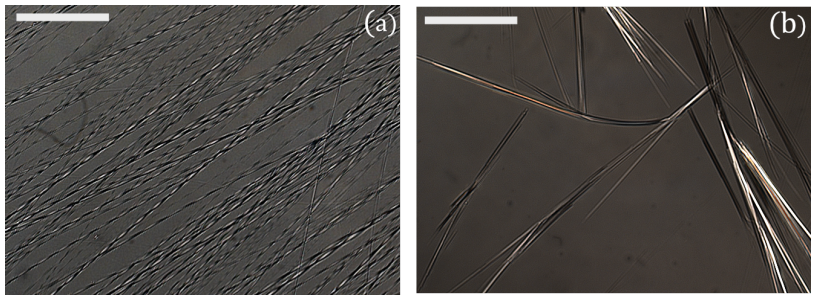

Figure 7.12: POM images between crossed polarising filters of 20 wt.% HSA gels in; (a) 1:1 decanoic acid : L-menthol; (b) 1:1 decanoic acid: thymol. The birefringent nature of the fibres is clearly seen, where twisted fibres are formed in (a) due to the chiral nature of the ES. The scale bar represents a length of 100 µm in both images.

served in the SAXS. Where gels were formed, peaks were observed in the SAXS at ≈0.135 $Å^{-1}$ and ≈0.400 $Å^{-1}$, with a weak reflection at 0.268 $Å^{-1}$ which is indicative of a lamellar bilayer structure. The peak at ≈0.135 $Å^{-1}$ was attributed to the head-to-head repeat distance of two HSA molecules dimerised at their carboxylic acid head groups. In some samples, there were low-q scattering features, which could be feasibly fitted to a parallelepiped model, as seen in Figure 7.13. The best fit results were achieved for a, b and c parameters of approximately 220 Å, 240 Å and 1350 Å, giving rectangular prisms which are a feasible for the high aspect ratio fibres observed in POM. These parallelepiped can be described by stacks of HSA fibres, sandwiched by ES layers between them. The close proximity of the solvent is also illustrated by the transfer of chiral nature of L-menthol containing ES to the fibres surrounded by it, forming the twisted fibres seen in POM.

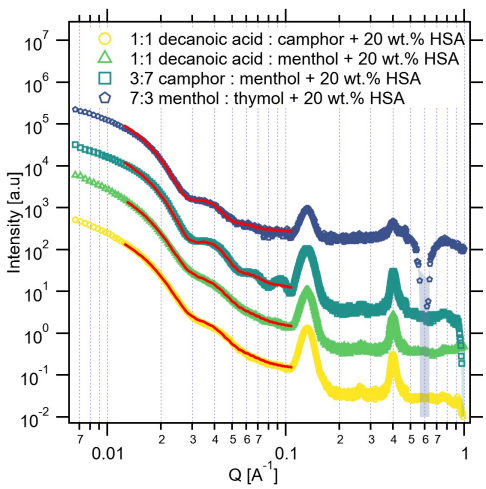

Figure 7.13: The SAXS data of 20 wt.% HSA in ES, with overlaid fits to the parallelepiped model. The plots and their respective fits have been offset along the y-axis for visual clarity.

As the HSA forms gel fibres which are affected by the hydrogen bonding nature of the ES, this is a fantastic candidate to study the varying hydrogen bonding environment of ES mixtures. This work not only contributes to the knowledge base surrounding HSA in various solvents, but also to the properties of eutectic mixtures and how their tunable properties can be exploited.

Conclusions and Outlook

To summarise this period of work, in a journey across the soft matter material chemistry landscape, many lessons have been learned. The work summarised in Paper I allowed for a interesting dive into designing microfluidic devices and integrating them into beamlines for effective use. With background studies into the mode of action of the current aluminium based antiperspirants, increased understanding of the current state of the art in terms of antiperspirant technology. Papers II and III have certainly added to the knowledge in the rapidly growing field around Type V (D)ES. Their use in emulsion systems stabilised with non-ionic surfactants is an intriguing contribution to this field, showing that these DES do have the potential to replace conventional oils and solvents. The work into eutectogels highlights the tunable behaviour of these ES mixtures and how flexible they are as a family of solvents. The findings within this thesis are interesting not only from applied science standpoint, but also contribute to the fundamental understanding of the capabilities of Type V (D)ES.

Future Work

The study into aluminium salts and a model protein in microfluidics in Paper I could lead to many interesting studies. If the internal surfaces of the microfluidic device were adapted to be more akin to physiological skin, the results would be much more reliable. If these developments were successfully paired with the high transmission microfluidic device, using the multi-layered approach, this could yield some very interesting results. Alternately, the knowledge gained from the microfluidic studies could be used to produce similar microfluidic devices to monitor reactions where the surface chemistry of the microfluidic channel is not so vital to the function of the device, for this there is seemingly infinite possibilities.

This work gained momentum towards the final stages of the project, which has produced much data which has not had time to develop into manuscripts. Therefore, there is immediately evident future prospects for more interesting

publications. Firstly, arising from Paper II, the interfacial structures formed at the emulsion interface were intriguing and led to further synchrotron experiments using a micro-focused X-ray beam on the I22 beamline, Diamond Light Source, UK. This work studied the interface of the bulk phases of the emulsions and observed the different surfactant structures formed across the interface of the two solutions as opposed to the dispersed system studied within this thesis.

With regard to Paper III, this work highlighted many interesting chemophysical properties of Type V ES, which is still a field rapidly growing in interest. The tunable properties of DES are always mentioned in the literature, but this study highlights how these DES can act as designer solvents. Immediately stemming from this work, the chiral nature of the DES on the HSA fibres is intriguing and certainly would make for an interesting TEM study into the effect of the DES chirality on the HSA fibrous structure.

References

[1] Boualem Hammouda. *The SANS Toolbox*. National Institute of Standards and Technology, Gaithersburg, 2016. URL `http://www.ncnr.nist.gov/staff/hammouda/the_SANS_toolbox.pdf`.

[2] D.S. Sivia. *Elementary Scattering Theory For X-ray and Neutron Users*. Oxford University Press, 2011.

[3] Cy M. Jeffries, Jan Ilavsky, Anne Martel, Stephan Hinrichs, Andreas Meyer, Jan Skov Pedersen, Anna V. Sokolova, and Dmitri I. Svergun. Small-angle x-ray and neutron scattering. *Nature Reviews Methods Primers*, 1(1), 2021. ISSN 2662-8449. doi: 10.1038/s43586-021-00064-9.

[4] V.F. Sears. Neutron scattering lengths and cross sections. *Neutron News*, 1992.

[5] Cecile A. Dreiss Vania Croce, Terence Cosgrove. Mixed spherical and wormlike micelles: A contrast-matching study by small-angle neutron scattering. *Langmuir*, 20:9978–9982, 2004.

[6] W. Muller, R. Schweins, B. Nocker, H. Egold, Y. Hannappel, and K. Huber. Sans contrast matching for the unambiguous localization of anionic dye in cationic surfactant micelles. *Nanoscale Adv*, 5(19):5367–5384, 2023. ISSN 2516-0230 (Electronic) 2516-0230 (Linking). doi: 10.1039/d3na00556a. URL `https://www.ncbi.nlm.nih.gov/pubmed/37767037`. Muller, Wenke Schweins, Ralf Nocker, Bernd Egold, Hans Hannappel, Yvonne Huber, Klaus eng England 2023/09/28 Nanoscale Adv. 2023 Sep 11;5(19):5367-5384. doi: 10.1039/d3na00556a. eCollection 2023 Sep 26.

[7] L. Poskin, L. Porcar, S. Prevost, R. Murphy, C. Michaux, and A. Martel. Nanodiscs formation process studied by contrast variation-sans. *Biochim Biophys Acta Biomembr*, 1868(3):184511, 2026. ISSN 1879-2642 (Electronic) 0005-2736 (Linking). doi: 10.1016/j.bbamem.2026.184511. URL `https://www.ncbi.nlm.nih.gov/pubmed/41763286`.

[8] Amy Y. Xu, Khaleda C. Rinee, Carrie Stemple, Maria Monica Castellanos, Kunal Bakshi, Susan Krueger, and Joseph E. Curtis. Counting the water: Characterize the hydration level of aluminum adjuvants using contrast matching small-angle neutron scattering. *Colloids and Surfaces A: Physicochemical and Engineering Aspects*, 648, 2022. ISSN 09277757. doi: 10.1016/j.colsurfa.2022.129285.

[9] R. G. Kirste, W. A. Kruse, and J. Schelten. Die bestimmung des trägheitsradius von polymethylmethacrylat im glaszustand durch neutronenbeugung. *Die Makromolekulare Chemie*, 164(1):343–343, 1973. ISSN 0025-116X. doi: https://doi.org/10.1002/macp.1973.021640130. URL `https://onlinelibrary.wiley.com/doi/abs/10.1002/macp.1973.021640130`.

[10] Von W. Freidrich, P. Knipping, and M. Laue. Interferenz-ersheinungen be röntgenstrahlen. *Sitzungsberichte der Bayerischen Akademie der Wissenschaften*, 1912.

[11] P. Krishnamurti. Studies in x-ray diffraction - part i. *Indian Journal of Physics*, pages 473–488, 1930.

[12] Jan Ilavsky, Pete R. Jemian, Andrew J. Allen, Fan Zhang, Lyle E. Levine, and Gabrielle G. Long. Ultra-small-angle x-ray scattering at the advanced photon source. *Journal of Applied Crystallography*, 42(3):469–479, 2009. ISSN 0021-8898. doi: 10.1107/s0021889809008802.

[13] Jan Ilavsky, Pete R. Jemian, Andrew J. Allen, Fan Zhang, Lyle E. Levine, and Gabrielle G. Long. Ultra-small-angle x-ray scattering at the advanced photon source. *Journal of Applied Crystallography*, 42(3):469–479, 2009. ISSN 0021-8898. doi: 10.1107/s0021889809008802.

[14] Albert C Thompson, David T Attwood, Malcolm R Howells, Jeffrey B Kortright, Arthur L Robinson, James H Underwood, Kwang-Je Kim, Janos Kirz, Ingolf Lindau, Piero Pianetta, Herman Winick, Gwyn P Williams, and James H Scofield. *X-Ray Data Booklet*. Lawrence Berkeley National Laboratory, University of California, 2009.

[15] Albert C Thompson, David T Attwood, Malcolm R Howells, Jeffrey B Kortright, Arthur L Robinson, James H Underwood, Kwang-Je Kim, Janos Kirz, Ingolf Lindau, Piero Pianetta, Herman Winick, Gwyn P Williams, and James H Scofield. *X-ray Data Booklet*. Lawrence Berkeley National Laboratory, University of California, 2009.

[16] A. J. Smith, S. G. Alcock, L. S. Davidson, J. H. Emmins, J. C. Hiller Bardsley, P. Holloway, M. Malfois, A. R. Marshall, C. L. Pizzey, S. E. Rogers, O. Shebanova, T. Snow, J. P. Sutter, E. P. Williams, and N. J. Terrill. I22: Saxs/waxs beamline at diamond light source - an overview of 10 years operation. *J Synchrotron Radiat*, 28(Pt 3):939–947, 2021. ISSN 1600-5775 (Electronic) 0909-0495 (Print) 0909-0495 (Linking). doi: 10.1107/S1600577521002113. URL `https://www.ncbi.nlm.nih.gov/pubmed/33950002`.

[17] UKRI. Sans2d, isis neuron and muon source. `https://www.isis.stfc.ac.uk/instruments/sans2d/`. Accessed: 13-04-2026.

[18] H. H. Reller and W. L. Luedders. Pharmaceutical and toxicological effects of topically applied agents on the eccrine sweat glands. *Advances in modern toxicology*, 4:18–54, 1977.

[19] R. P. Quatrale, A. H. Waldman, J. G. Rogers, and C. B. Felger. The mechanism of antiperspirant action by aluminium salts. the effect of cellophane tape stripping on aluminium salt-inhibited eccrine sweat glands. *Journal of the Society of Cosmetic Chemistry*, 32:67–73, 1981.

[20] G. K. Menon, G. W. Cleary, and M. E. Lane. The structure and function of the stratum corneum. *Int J Pharm*, 435(1):3–9, 2012. ISSN 1873-3476 (Electronic) 0378-5173 (Linking). doi: 10.1016/j.ijpharm.2012.06.005. URL `https://www.ncbi.nlm.nih.gov/pubmed/22705878`. Menon, Gopinathan K Cleary, Gary W Lane, Majella E eng Review Netherlands Int J Pharm. 2012 Oct 1;435(1):3-9. doi: 10.1016/j.ijpharm.2012.06.005. Epub 2012 Jun 15.

[21] E. Holzle and O. Braun-Falco. Structural changes in axillary eccrine glands following long-term treatment with aluminium chloride hexahydrate solution. *British Journal of Dermatology*, 110:339–403, 1984.

[22] A. Bretagne, F. Cotot, M. Arnaud-Roux, M. Sztucki, B. Cabane, and J. B. Galey. The mechanism of eccrine sweat pore plugging by aluminium salts using microfluidics combined with small angle x-ray scattering. *Soft Matter*, 13(20):3812–3821, 2017. ISSN 1744-6848 (Electronic) 1744-683X (Linking). doi: 10.1039/c6sm02510b. URL `https://www.ncbi.nlm.nih.gov/pubmed/28485735`.

[23] J. B. Galey, R. Botet, Y. Sakhawoth, J. Dupire, F. Leonforte, M. Chardon, F. Monti, P. Tabeling, and B. Cabane. Dendritic growth of protein gel in the course of sweat pore plugging by aluminium salts under physiological conditions. *Soft Matter*, 17(35):8022–8026, 2021. ISSN 1744-6848

(Electronic) 1744-683X (Linking). doi: 10.1039/d1sm01029h. URL https://www.ncbi.nlm.nih.gov/pubmed/34525157.

[24] Y. Sakhawoth, J. Dupire, F. Leonforte, M. Chardon, F. Monti, P. Tabeling, B. Cabane, R. Botet, and J. B. Galey. Real time observation of the interaction between aluminium salts and sweat under microfluidic conditions. *Sci Rep*, 11(1):6376, 2021. ISSN 2045-2322 (Electronic) 2045-2322 (Linking). doi: 10.1038/s41598-021-85691-8. URL https://www.ncbi.nlm.nih.gov/pubmed/33737654.

[25] A.W. Stillians. The control of localized hyperhidrosis. *JAMA*, 67:2015–2016, 1916.

[26] Carl N. Andersen and Briarcliff Manor. Aluminium chlorohydrate astringent, 20.12.1949 1949.

[27] Dirk L. Teagarden, John F. Kozlowski, Joe L. White, and Stanley L. Hem. Aluminum chlorohydrate i: Structure studies. *Journal of Pharmaceutical Sciences*, 70(7), 1981.

[28] Long Pan. Method of making an antiperspirant active composition having sec chromatogram exhibiting high sec peak 4 intensity, 2012.

[29] William V. Rausch and Harold D. Bale. Small-angle x-ray scattering from hydrolyzed aluminum nitrate solutions. *The Journal of Chemical Physics*, 40(11):3391–3394, 1964. ISSN 0021-9606 1089-7690. doi: 10.1063/1.1725011.

[30] N. Ouadah, C. Moire, J. F. Kuntz, F. Brothier, and H. Cottet. Analysis and characterization of aluminum chlorohydrate oligocations by capillary electrophoresis. *J Chromatogr A*, 1492:144–150, 2017. ISSN 1873-3778 (Electronic) 0021-9673 (Linking). doi: 10.1016/j.chroma.2017.02.008. URL https://www.ncbi.nlm.nih.gov/pubmed/28284762. Ouadah, Nesrine Moire, Claudine Kuntz, Jean-Francois Brothier, Fabien Cottet, Herve eng Netherlands J Chromatogr A. 2017 Apr 7;1492:144-150. doi: 10.1016/j.chroma.2017.02.008. Epub 2017 Feb 6.

[31] B. L. Phillips, J. S. Vaughn, S. Smart, and L. Pan. Characterization of al30 in commercial poly-aluminum chlorohydrate by solid-state (27)al nmr spectroscopy. *Journal of Colloid Interface Science*, 476:230–239, 2016. ISSN 1095-7103 (Electronic) 0021-9797 (Linking). doi: 10.1016/j.jcis.2016.05.019. URL https://www.ncbi.nlm.nih.gov/pubmed/27232539.

[32] C. Scherer, Jeffrey Brinker, and George W. *The Physics and Chemistry of Sol-Gel Processing*. Elsevier Science, 1990. ISBN 0-12-134970-5.

[33] Y. Cardona, S. A. Korili, and A. Gil. Understanding the formation of al13 and al30 polycations to the development of microporous materials based on al13-and al30-pilc montmorillonites: a review. *Applied Clay Science*, 2021. doi: 10.1016/j.clay.2021.105996.

[34] Baes and Mesmer. *The Hydrolysis of Cations*. Wiley, 1976.

[35] J.W Akitt and A. Farthing. Aluminium-27 nuclear magnetic resonance studies of the hydrolysis of aluminium(iii). part 4. hydrolysis using sodium carbonate. *Journal of Chemical Society*, pages 1617–1623, 1981.

[36] L. Baker and J Figgis. A new fundamental type of inorganic complex: Hybrid between heteropoly and conventional coordination complexes. possibilities for geometrical isomerisms in 11-, 12-, 17-, and 18-heteropoly derivatives. *American Chemical Society*, 92:3794–3797, 1970.

[37] William H. Casey. Large aqueous aluminium hydroxide molecules. *Chemical Reviews*, 106, 2006.

[38] Shaotang Yuan, John Vaughn, Iraklis Pappas, Michael Fitzgerald, James G. Masters, and Long Pan. Optimal aluminium/zirconium: Protein interactions for predicting antiperspirant efficacy using zeta potential measurements. *Journal of Cosmetic Science*, 66:95–111, 2015.

[39] IFCC. Antiperspirants and deodorants: Principles of underarm technology, 1998.

[40] E. Cross. Ap actives, 2021.

[41] D. Chin and R. Achari. Analysis of glycine in antiperspirant products by hplc. *Journal of the Society of Cosmetic Chemistry*, 33:359–362, 1982.

[42] L. Pan, R. Heddy, J. Li, C. Zheng, X. Y. Huang, X. Tang, and L. Kilpatrick. Synthesis and structural determination of a hexanuclear zirconium glycine compound formed in aqueous solution. *Inorg Chem*, 47(13):5537–9, 2008. ISSN 1520-510X (Electronic) 0020-1669 (Linking). doi: 10.1021/ic800292e. URL `https://www.ncbi.nlm.nih.gov/pubmed/18512904`.

[43] Iraklis Pappas, Michael Fitzgerald, Xiao-Ying Huang, Jing Li, and Long Pan. Thermally resolved in situ dynamic light scattering studies of zirconium(iv) complex formation. *Crystal Growth & Design*, 9(12):5213–5219, 2009. ISSN 1528-7483 1528-7505. doi: 10.1021/cg900681x.

[44] Thaddeus Bartter, Richard S. Irwin, Jerrold L. Abraham, Andre Dascal, Gerald Nash, Jay S. Himmelstein, and Peter J. Jederlinic. Zirconium compound-induced pulmonary fibrosis. *Archives of Internal Medicine*, 151: 1997–1201, 1991.

[45] M. A. Buttkewitz, C. Heuer, and J. Bahnemann. Sensor integration into microfluidic systems: trends and challenges. *Curr Opin Biotechnol*, 83: 102978, 2023. doi: 10.1016/j.copbio.2023.102978. URL `https://www.ncbi.nlm.nih.gov/pubmed/37531802`.

[46] K. Y. Chumbimuni-Torres, R. E. Coronado, A. M. Mfuh, C. Castro-Guerrero, M. F. Silva, G. R. Negrete, R. Bizios, and C. D. Garcia. Adsorption of proteins to thin-films of pdms and its effect on the adhesion of human endothelial cells. *RSC Adv*, 1(4):706–714, 2011. doi: 10.1039/C1RA00198A. URL `https://www.ncbi.nlm.nih.gov/pubmed/25068038`.

[47] Mark A. Levenstein, Clara Anduix-Canto, Yi-Yeoun Kim, Mark A. Holden, Carlos González Niño, David C. Green, Stephanie E. Foster, Alexander N. Kulak, Lata Govada, Naomi E. Chayen, Sarah J. Day, Chiu C. Tang, Britta Weinhausen, Manfred Burghammer, Nikil Kapur, and Fiona C. Meldrum. Droplet microfluidics xrd identifies effective nucleating agents for calcium carbonate. *Advanced Functional Materials*, 29 (19), 2019. doi: 10.1002/adfm.201808172.

[48] M. A. Levenstein, C. Chevallard, F. Malloggi, F. Testard, and O. Tache. Micro- and milli-fluidic sample environments for in situ x-ray analysis in the chemical and materials sciences. *Lab Chip*, 25(5):1169–1227, 2025. doi: 10.1039/d4lc00637b. URL `https://www.ncbi.nlm.nih.gov/pubmed/39775751`.

[49] Agathe Fournier. *Interactions of Pure Aluminium Hydrolytic Species - Keggin Polyoxocations and hydroxide with Biologically relevant molecules*. Thesis, School of Biomedical and Natural Sciences, 2008.

[50] Nnyigide Osita Sunday, Oh Yuna, Song Hyeong Yong, Park Eun-Kyoung, Choi Soo-Hyung, and Hyun Kyu. Effect of urea on heat-induced gelation of bovine serum albumin (bsa) studied by rheology and small angle neutron scattering (sans). *Korea-australia Rheology Journal*, 2017. doi: 10.1007/s13367-017-0012-4. URL `https://doi.org/10.1007/s13367-017-0012-4`.

[51] Z. Sonner, E. Wilder, J. Heikenfeld, G. Kasting, F. Beyette, D. Swaile, F. Sherman, J. Joyce, J. Hagen, N. Kelley-Loughnane, and R. Naik.

The microfluidics of the eccrine sweat gland, including biomarker partitioning, transport, and biosensing implications. *Biomicrofluidics*, 9(3): 031301, 2015. ISSN 1932-1058 (Print) 1932-1058 (Linking). doi: 10.1063/1.4921039. URL https://www.ncbi.nlm.nih.gov/pubmed/26045728.

[52] A. P. Abbott, G. Capper, D. L. Davies, R. K. Rasheed, and V. Tambyrajah. Novel solvent properties of choline chloride/urea mixtures. *Chem Commun (Camb)*, pages 70–1, 2003. ISSN 1359-7345 (Print) 1359-7345 (Linking). doi: 10.1039/b210714g. URL https://www.ncbi.nlm.nih.gov/pubmed/12610970.

[53] Frederick Guthrie. Lii. on eutexia. *The London, Edinburgh, and Dublin Philosophical Magazine and Journal of Science*, 17(108):462–482, 1884. ISSN 1941-5982. doi: 10.1080/14786448408627543. URL https://doi.org/10.1080/14786448408627543.

[54] A. P. Abbott, G. Capper, D. L. Davies, H. L. Munro, R. K. Rasheed, and V. Tambyrajah. Preparation of novel, moisture-stable, lewis-acidic ionic liquids containing quaternary ammonium salts with functional side chains. *Chem Commun (Camb)*, pages 2010–1, 2001. ISSN 1359-7345 (Print) 1359-7345 (Linking). doi: 10.1039/b106357j. URL https://www.ncbi.nlm.nih.gov/pubmed/12240264.

[55] Xiangqian Meng, Karine Ballerat-Busserolles, Pascale Husson, and Jean-Michel Andanson. Impact of water on the melting temperature of urea + choline chloride deep eutectic solvent. *New Journal of Chemistry*, 40(5): 4492–4499, 2016. ISSN 1144-0546 1369-9261. doi: 10.1039/c5nj02677f.

[56] E. L. Smith, A. P. Abbott, and K. S. Ryder. Deep eutectic solvents (dess) and their applications. *Chem Rev*, 114(21):11060–82, 2014. ISSN 1520-6890 (Electronic) 0009-2665 (Linking). doi: 10.1021/cr300162p. URL https://www.ncbi.nlm.nih.gov/pubmed/25300631.

[57] D. O. Abranches and J. A. P. Coutinho. Everything you wanted to know about deep eutectic solvents but were afraid to be told. *Annu Rev Chem Biomol Eng*, 14:141–163, 2023. ISSN 1947-5446 (Electronic) 1947-5438 (Linking). doi: 10.1146/annurev-chembioeng-101121-085323. URL https://www.ncbi.nlm.nih.gov/pubmed/36888992.

[58] Z. Lei, B. Chen, Y. M. Koo, and D. R. MacFarlane. Introduction: Ionic liquids. *Chem Rev*, 117(10):6633–6635, 2017. ISSN 1520-6890 (Electronic) 0009-2665 (Linking). doi: 10.1021/acs.chemrev.7b00246. URL https://www.ncbi.nlm.nih.gov/pubmed/28535681.

[59] Mónia A. R. Martins, Simão P. Pinho, and João A. P. Coutinho. Insights into the nature of eutectic and deep eutectic mixtures. *Journal of Solution Chemistry*, 48(7):962–982, 2018. ISSN 0095-9782 1572-8927. doi: 10.1007/s10953-018-0793-1.

[60] John C. Warner, Amy S. Cannon, and Kevin M. Dye. Green chemistry. *Environmental Impact Assessment Review*, 24(7-8):775–799, 2004. ISSN 01959255. doi: 10.1016/j.eiar.2004.06.006.

[61] Verena Huber, Katharina Häckl, Didier Touraud, and Werner Kunz. Natural deep eutectic solvents: From simple systems to complex colloidal mixtures. *Eutectic Solvents and Stress in Plants*, page 17–40, 2021. ISSN 9780128216910. doi: 10.1016/bs.abr.2020.09.001.

[62] Iqra Batool, Shafaq Nisar, Lamia Hamrouni, and Muhammad Idrees Jilani. Extraction, production and analysis techniques for menthol: A review. *International Journal of Chemical and Biochemical Sciences*, 14: 71–76, 2018.

[63] Regina Klein, Eva Müller, Birgit Kraus, Gabi Brunner, Boris Estrine, Didier Touraud, Jörg Heilmann, Matthias Kellermeier, and Werner Kunz. Biodegradability and cytotoxicity of choline soaps on human cell lines: effects of chain length and the cation. *RSC Advances*, 3(45), 2013. ISSN 2046-2069. doi: 10.1039/c3ra42812e.

[64] Mónia A. R. Martins, Emanuel A. Crespo, Paula V. A. Pontes, Liliana P. Silva, Mark Bülow, Guilherme J. Maximo, Eduardo A. C. Batista, Christoph Held, Simão P. Pinho, and João A. P. Coutinho. Tunable hydrophobic eutectic solvents based on terpenes and monocarboxylic acids. *ACS Sustainable Chemistry & Engineering*, 6(7):8836–8846, 2018. ISSN 2168-0485 2168-0485. doi: 10.1021/acssuschemeng.8b01203.

[65] Y. Chen, D. Yu, W. Chen, L. Fu, and T. Mu. Water absorption by deep eutectic solvents. *Phys Chem Chem Phys*, 21(5):2601–2610, 2019. doi: 10.1039/c8cp07383j. URL `https://www.ncbi.nlm.nih.gov/pubmed/30657495`.

[66] L. V. Tavares Duarte de Alencar, S. B. Rodriguez-Reartes, F. W. Tavares, and F. Llovell. Assessing viscosity in sustainable deep eutectic solvents and cosolvent mixtures: An artificial neural network-based molecular approach. *ACS Sustain Chem Eng*, 12(21):7987–8000, 2024. doi: 10.1021/acssuschemeng.3c07219. URL `https://www.ncbi.nlm.nih.gov/pubmed/38817974`.

[67] Dannie J. G. P. van Osch, Carin H. J. T. Dietz, Jaap van Spronsen, Maaike C. Kroon, Fausto Gallucci, Martin van Sint Annaland, and Remco Tuinier. A search for natural hydrophobic deep eutectic solvents based on natural components. *ACS Sustainable Chemistry & Engineering*, 7(3): 2933–2942, 2019. ISSN 2168-0485 2168-0485. doi: 10.1021/acssuschemeng.8b03520.

[68] S.R Euston and R.L Hirst. The emulsifying properties of commercial milk protein products in simple oil-in-water emulsions and in a model food system. *Food Chemistry and Toxicology*, 65:934–940, 2000.

[69] Surajudeen Abdulsalam. Production of emulsion house paint using polyvinyl acetate and gum arabic as binder. *International Journal of Materials Science and Applications*, 4(5), 2015. ISSN 2327-2635. doi: 10.11648/j.ijmsa.20150405.20.

[70] D. Venkataramani, A. Tsulaia, and S. Amin. Fundamentals and applications of particle stabilized emulsions in cosmetic formulations. *Adv Colloid Interface Sci*, 283:102234, 2020. doi: 10.1016/j.cis.2020.102234. URL `https://www.ncbi.nlm.nih.gov/pubmed/32795669`.

[71] Anika Söldner, Julia Zach, and Burkhard König. Deep eutectic solvents as extraction media for metal salts and oxides exemplarily shown for phosphates from incinerated sewage sludge ash. *Green Chemistry*, 21(2):321–328, 2019. ISSN 1463-9262 1463-9270. doi: 10.1039/c8gc02702a.

[72] T. Arnold, A. J. Jackson, A. Sanchez-Fernandez, D. Magnone, A. E. Terry, and K. J. Edler. Surfactant behavior of sodium dodecylsulfate in deep eutectic solvent choline chloride/urea. *Langmuir*, 31(47):12894–902, 2015. ISSN 1520-5827 (Electronic) 0743-7463 (Linking). doi: 10.1021/acs.langmuir.5b02596. URL `https://www.ncbi.nlm.nih.gov/pubmed/26540438`.

[73] Elly K. Bathke, Daniel T. Bowron, Iva Manasi, and Karen J. Edler. The influence of chirality on the structure of a tartaric acid-choline chloride deep eutectic solvent. *Journal of Molecular Liquids*, 402, 2024. ISSN 01677322. doi: 10.1016/j.molliq.2024.124735.

[74] Oliver S. Hammond, Daniel T. Bowron, and Karen J. Edler. Liquid structure of the choline chloride-urea deep eutectic solvent (reline) from neutron diffraction and atomistic modelling. *Green Chemistry*, 18(9):2736–2744, 2016. ISSN 1463-9262 1463-9270. doi: 10.1039/c5gc02914g.

[75] O. S. Hammond, D. T. Bowron, and K. J. Edler. The effect of water upon deep eutectic solvent nanostructure: An unusual transition from ionic mixture to aqueous solution. *Angew Chem Int Ed Engl*, 56(33): 9782–9785, 2017. ISSN 1521-3773 (Electronic) 1433-7851 (Print) 1433-7851 (Linking). doi: 10.1002/anie.201702486. URL `https://www.ncbi.nlm.nih.gov/pubmed/28480595`.

[76] Oliver S. Hammond, Adrian Sanchez-Fernandez, Rachel Tyte, Robert Dalgliesh, Andrew J. Smith, and Karen J. Edler. Mix-and-match diols: Adjusting self-assembly of micellar phases in choline chloride eutectics. *Crystals*, 12(11), 2022. ISSN 2073-4352. doi: 10.3390/cryst12111621.

[77] A. Pandey, R. Rai, M. Pal, and S. Pandey. How polar are choline chloride-based deep eutectic solvents? *Phys Chem Chem Phys*, 16(4):1559–68, 2014. ISSN 1463-9084 (Electronic) 1463-9076 (Linking). doi: 10.1039/c3cp53456a. URL `https://www.ncbi.nlm.nih.gov/pubmed/24305780`.

[78] O. Dlugosz. Natural deep eutectic solvents in the synthesis of inorganic nanoparticles. *Materials (Basel)*, 16(2), 2023. ISSN 1996-1944 (Print) 1996-1944 (Electronic) 1996-1944 (Linking). doi: 10.3390/ma16020627. URL `https://www.ncbi.nlm.nih.gov/pubmed/36676363`.

[79] Amos Dwamena. Recent advances in hydrophobic deep eutectic solvents for extraction. *Separations*, 6(1), 2019. ISSN 2297-8739. doi: 10.3390/separations6010009.

[80] Jinxiao Dou, Shaoyu Wang, Yueying Li, Hua Li, Xingxing Chen, and Jianglong Yu. Toxic gas removal using deep eutectic solvents: A review of fundamentals and applications. *Fuel*, 420, 2026. ISSN 00162361. doi: 10.1016/j.fuel.2026.138947.

[81] Giselle de Araujo Lima e Souza, Emilia Pelegano-Titmuss, Miguel Muñoz, Burcu Gurkan, Maria Enrica di Pietro, Andrea Mele, Phillip Stallworth, and Steven Greenbaum. Probing the potential of type v deep eutectic solvents as sustainable electrolytes. *Journal of Molecular Liquids*, 416, 2024. ISSN 01677322. doi: 10.1016/j.molliq.2024.126526.

[82] J. C. Araque, J. J. Hettige, and C. J. Margulis. Modern room temperature ionic liquids, a simple guide to understanding their structure and how it may relate to dynamics. *J Phys Chem B*, 119(40):12727–40, 2015. ISSN 1520-5207 (Electronic) 1520-5207 (Linking). doi: 10.1021/acs.jpcb.5b05506. URL `https://www.ncbi.nlm.nih.gov/pubmed/26244375`.

[83] Yuta Araki, Yuma Hamada, Norika Imamura, Koki Yamasaka, and Mina Sakuragi. Evaluation of terpene-based hydrophobic deep eutectic solvents as skin permeation enhancers. *Japanese Journal of Applied Physics*, 62 (1), 2023. ISSN 0021-4922 1347-4065. doi: 10.35848/1347-4065/acb392.

[84] S. J. Bryant, M. A. da Silva, K. M. Z. Hossain, V. Calabrese, J. L. Scott, and K. J. Edler. Deep eutectic solvent in water pickering emulsions stabilised by cellulose nanofibrils. *RSC Adv*, 10(61):37023–37027, 2020. ISSN 2046-2069 (Electronic) 2046-2069 (Linking). doi: 10.1039/d0ra07575b. URL `https://www.ncbi.nlm.nih.gov/pubmed/35521254`.

[85] Usman T. Syed, Inês C. Leonardo, Gracia Mendoza, Frédéric B. Gaspar, Enrique Gámez, Rosa M. Huertas, Maria T. B. Crespo, Manuel Arruebo, João G. Crespo, Victor Sebastian, and Carla Brazinha. On the role of components of therapeutic hydrophobic deep eutectic solvent-based nanoemulsions sustainably produced by membrane-assisted nanoemulsification for enhanced antimicrobial activity. *Separation and Purification Technology*, 285, 2022. ISSN 13835866. doi: 10.1016/j.seppur.2021.120319.

[86] Usman T. Syed, Inês Leonardo, Ruth Lahoz, Frédéric B. Gaspar, Rosa Huertas, Maria T. B. Crespo, Manuel Arruebo, J. G. Crespo, Victor Sebastian, and Carla Brazinha. Microengineered membranes for sustainable production of hydrophobic deep eutectic solvent-based nanoemulsions by membrane emulsification for enhanced antimicrobial activity. *ACS Sustainable Chemistry & Engineering*, 8(44):16526–16536, 2020. ISSN 2168-0485 2168-0485. doi: 10.1021/acssuschemeng.0c05612.

[87] Dannie J. G. P. van Osch, Lawien F. Zubeir, Adriaan van den Bruinhorst, Marisa A. A. Rocha, and Maaike C. Kroon. Hydrophobic deep eutectic solvents as water-immiscible extractants. *Green Chemistry*, 17(9):4518–4521, 2015. ISSN 1463-9262 1463-9270. doi: 10.1039/c5gc01451d.

[88] N. Schaeffer, I. C. M. Vaz, M. S. Pinheiro, F. Olea, T. Hanada, S. Dourdain, and J. A. P. Coutinho. Examining the potential of type v dess for the solvent extraction of metal ions. *Green Chem*, 27(17): 4438–4463, 2025. ISSN 1463-9262 (Print) 1463-9262 (Electronic) 1463-9262 (Linking). doi: 10.1039/d5gc00489f. URL `https://www.ncbi.nlm.nih.gov/pubmed/40206710`.

[89] P. Makos, A. Przyjazny, and G. Boczkaj. Hydrophobic deep eutectic solvents as "green" extraction media for polycyclic aromatic hydrocarbons in aqueous samples. *J Chromatogr A*, 1570:28–37, 2018. ISSN 1873-3778 (Electronic) 0021-9673 (Linking). doi: 10.1016/j.chroma.2018.07.070. URL `https://www.ncbi.nlm.nih.gov/pubmed/30082124`.

[90] Taylan Topal, Asli Card, Andrew D. Mackenzie, Kirill Lagutin, Susan N. Marshall, Adam H. Cumming, and Daniel P. Killeen. Hydrophobic natural deep eutectic solvents for marine lipid extraction. *Journal of the American Oil Chemists' Society*, 101(3):361–367, 2023. ISSN 0003-021X 1558-9331. doi: 10.1002/aocs.12757.

[91] M. Li, J. Yuan, Z. Liu, T. Yin, and C. Peng. Multifunctional deep eutectic solvent-based microemulsion for transdermal delivery of artemisinin. *Langmuir*, 40(10):5098–5105, 2024. ISSN 1520-5827 (Electronic) 0743-7463 (Linking). doi: 10.1021/acs.langmuir.3c02748. URL `https://www.ncbi.nlm.nih.gov/pubmed/38412279`.

[92] Chaoxi Zeng, Yugang Liu, Zemin Ding, Huiping Xia, and Shiyin Guo. Physicochemical properties and antibacterial activity of hydrophobic deep eutectic solvent-in-water nanoemulsion. *Journal of Molecular Liquids*, 338, 2021. ISSN 01677322. doi: 10.1016/j.molliq.2021.116950.

[93] J. M. Silva, C. V. Pereira, F. Mano, E. Silva, V. I. B. Castro, I. Sa-Nogueira, R. L. Reis, A. Paiva, A. A. Matias, and A. R. C. Duarte. Therapeutic role of deep eutectic solvents based on menthol and saturated fatty acids on wound healing. *ACS Appl Bio Mater*, 2(10):4346–4355, 2019. ISSN 2576-6422 (Electronic) 2576-6422 (Linking). doi: 10.1021/acsabm.9b00598. URL `https://www.ncbi.nlm.nih.gov/pubmed/32030369`.

[94] Yael Kaplun-Frischoff and Elka Touitou. Testosterone skin permeation enhancement by menthol through formation of eutectic with drug and interaction with skin lipids. *Journal of Pharmaceutical Sciences*, 86 (12):1394–1399, 1997. ISSN 0022-3549. doi: https://doi.org/10.1021/js9701465. URL `https://www.sciencedirect.com/science/article/pii/S0022354915504620`.

[95] Paul W. Stott, Adrian C. Williams, and Brian W. Barry. Transdermal delivery from eutectic systems: enhanced permeation of a model drug, ibuprofen. *Journal of Controlled Release*, 50(1):297–308, 1998. ISSN 0168-3659. doi: https://doi.org/10.1016/S0168-3659(97)00153-3. URL `https://www.sciencedirect.com/science/article/pii/S0168365997001533https://www.sciencedirect.com/science/article/pii/S0168365997001533?via%3Dihub`.

[96] A. Manova, J. Viktorova, J. Kohler, S. Theiler, H. Keul, A. A. Piryazev, D. A. Ivanov, L. Tsarkova, and M. Moller. Multilamellar thermoresponsive emulsions stabilized with biocompatible semicrystalline block copolymers. *ACS Macro Lett*, 5(2):163–167, 2016. doi: 10.1021/acsmacrolett.5b00743. URL `https://www.ncbi.nlm.nih.gov/pubmed/35614692`.

[97] Qingchun Yuan, Olivier J. Cayre, Mohamed Manga, Richard A. Williams, and Simon Biggs. Preparation of particle-stabilized emulsions using membrane emulsification. *Soft Matter*, 6(7), 2010. ISSN 1744-683X 1744-6848. doi: 10.1039/b921372d.

[98] Ahmed Taha, Eman Ahmed, Amr Ismaiel, Muthupandian Ashokkumar, Xiaoyun Xu, Siyi Pan, and Hao Hu. Ultrasonic emulsification: An overview on the preparation of different emulsifiers-stabilized emulsions. *Trends in Food Science & Technology*, 105:363–377, 2020. ISSN 09242244. doi: 10.1016/j.tifs.2020.09.024.

[99] Dannie J. G. P. van Osch, J. van Spronsen, A. C. C. Esteves, R. Tuinier, and M. Vis. Oil-in-water emulsions based on hydrophobic eutectic systems. *Phys Chem Chem Phys*, 22(4):2181–2187, 2020. ISSN 1463-9084 (Electronic) 1463-9076 (Linking). doi: 10.1039/c9cp06762k. URL `https://www.ncbi.nlm.nih.gov/pubmed/31912861`.

[100] Nozomi Higashide, Nobuyuki Matsuda, Kazumitsu Naoe, and Masanao Imai. Application of food-grade magnesium stearate microparticles as stabilizer in preparation of biocompatible pickering emulsions. *Chemical Papers*, 75(4):1639–1648, 2020. ISSN 2585-7290 1336-9075. doi: 10.1007/s11696-020-01428-3.

[101] R. Xie, Z. Tan, W. Fan, J. Qin, S. Guo, H. Xiao, and Z. Tang. Deep-eutectic-solvent-in-water pickering emulsions stabilized by starch nanoparticles. *Foods*, 13(14), 2024. ISSN 2304-8158 (Print) 2304-8158 (Electronic) 2304-8158 (Linking). doi: 10.3390/foods13142293. URL `https://www.ncbi.nlm.nih.gov/pubmed/39063377`.

[102] R. Xie, Z. Tan, W. Fan, J. Qin, S. Guo, H. Xiao, and Z. Tang. Deep-eutectic-solvent-in-water pickering emulsions stabilized by starch nanoparticles. *Foods*, 13(14), 2024. doi: 10.3390/foods13142293. URL `https://www.ncbi.nlm.nih.gov/pubmed/39063377`.

[103] Jacob N. Israelachvili. *Intermolecular and Surface Forces*. Academic Press, University of California, Santa Barbara, California, USA, 3 edition, 2011. ISBN 9780123751829. doi: https://doi.org/10.1016/C2011-0-05119-0.

[104] A. Oshiro, D. C. da Silva, J. C. de Mello, V. W. de Moraes, L. P. Cavalcanti, M. K. Franco, M. I. Alkschbirs, L. F. Fraceto, F. Yokaichiya, T. Rodrigues, and D. R. de Araujo. Pluronics f-127/l-81 binary hydrogels as drug-delivery systems: influence of physicochemical aspects on release kinetics and cytotoxicity. *Langmuir*, 30(45):13689–98, 2014. doi: 10.1021/la503021c.

[105] Juan Albano, Damian Grillo, Julio Facelli, Marta Ferraro, and Mónica Pickholz. Study of the lamellar and micellar phases of pluronic f127: A molecular dynamics approach. *Processes*, 7(9), 2019. ISSN 2227-9717. doi: 10.3390/pr7090606.

[106] I. Grillo, I. Morfin, and S. Prevost. Structural characterization of pluronic micelles swollen with perfume molecules. *Langmuir*, 34(44):13395–13408, 2018. ISSN 1520-5827 (Electronic) 0743-7463 (Linking). doi: 10.1021/acs.langmuir.8b03050. URL `https://www.ncbi.nlm.nih.gov/pubmed/30350691`.

[107] E. J. Ricci, M. V. Bentley, M. Farah, R. E. Bretas, and J. M. Marchetti. Rheological characterization of poloxamer 407 lidocaine hydrochloride gels. *Eur J Pharm Sci*, 17(3):161–7, 2002. doi: 10.1016/s0928-0987(02)00166-5. URL `https://www.ncbi.nlm.nih.gov/pubmed/12393144`.

[108] G. Wanka, H. Hoffman, and W. Ulbricht. Phase diagrams and aggregation behavior of poly(oxyethylene)-poly(oxypropylene)-poly(oxyethylene)triblock copolymers in aqueous solutions. *Macromolecules*, 27:4145–4159, 1994. doi: 10.1021/ma00093a016.

[109] P. Zarrintaj, J. D. Ramsey, A. Samadi, Z. Atoufi, M. K. Yazdi, M. R. Ganjali, L. M. Amirabad, E. Zangene, M. Farokhi, K. Formela, M. R. Saeb, M. Mozafari, and S. Thomas. Poloxamer: A versatile tri-block copolymer for biomedical applications. *Acta Biomater*, 110:37–67, 2020. ISSN 1878-7568 (Electronic) 1742-7061 (Linking). doi: 10.1016/j.actbio.2020.04.028. URL `https://www.ncbi.nlm.nih.gov/pubmed/32417265`.

[110] M. S. Akash and K. Rehman. Recent progress in biomedical applications of pluronic (pf127): Pharmaceutical perspectives. *J Control Release*, 209:120–38, 2015. ISSN 1873-4995 (Electronic) 0168-3659 (Linking). doi: 10.1016/j.jconrel.2015.04.032. URL `https://www.ncbi.nlm.nih.gov/pubmed/25921088`.

[111] C. Ju, J. Sun, P. Zi, X. Jin, and C. Zhang. Thermosensitive micelles-hydrogel hybrid system based on poloxamer 407 for localized delivery of paclitaxel. *J Pharm Sci*, 102(8):2707–17, 2013. doi: 10.1002/jps.23649.

[112] S. D. Singh-Joy and V. C. McLain. Safety assessment of poloxamers 101, 105, 108, 122, 123, 124, 181, 182, 183, 184, 185, 188, 212, 215, 217, 231, 234, 235, 237, 238, 282, 284, 288, 331, 333, 334, 335, 338, 401, 402, 403, and 407, poloxamer 105 benzoate, and poloxamer 182 dibenzoate as used in cosmetics. *Int J Toxicol*, 27 Suppl 2:93–128, 2008. doi: 10.1080/10915810802244595.

[113] D. Wang and J. Hao. Self-assembly fibrillar network gels of simple surfactants in organic solvents. *Langmuir*, 27(5):1713–7, 2011. ISSN 1520-5827 (Electronic) 0743-7463 (Linking). doi: 10.1021/la104333x. URL https://www.ncbi.nlm.nih.gov/pubmed/21214186.

[114] Qi Wang. *Formation and Structure of Acid Soap Crystals through in-situ Neutralisation in the Environments of Surfactant*. Thesis, School of Chemical and Process Engineering, 2019.

[115] C. Florindo, L. G. Celia-Silva, L. F. G. Martins, L. C. Branco, and I. M. Marrucho. Supramolecular hydrogel based on a sodium deep eutectic solvent. *Chem Commun (Camb)*, 54(54):7527–7530, 2018. ISSN 1364-548X (Electronic) 1359-7345 (Linking). doi: 10.1039/c8cc03266a. URL https://www.ncbi.nlm.nih.gov/pubmed/29926055.

[116] Li-Sheng Hao, Cheng Yuan, Hong-Liang Zhong, Jing-Wei Ling, Han-Xiao Wang, and Yan-Qing Nan. Triple-stimuli-responsive hydrogels based on an aqueous mixed sodium stearate and cetyltrimethylammonium bromide system. *Journal of Molecular Liquids*, 364, 2022. ISSN 01677322. doi: 10.1016/j.molliq.2022.120010.

[117] Hai-Kuan Yang, Chen Zhang, Xiang-Ning He, and Pin-You Wang. Effects of alkyl chain lengths on 12-hydroxystearic acid derivatives based supramolecular organogels. *Colloids and Surfaces A: Physicochemical and Engineering Aspects*, 616, 2021. ISSN 09277757. doi: 10.1016/j.colsurfa.2021.126319.

[118] D. J. Adams. Personal perspective on understanding low molecular weight gels. *J Am Chem Soc*, 144(25):11047–11053, 2022. ISSN 1520-5126 (Electronic) 0002-7863 (Print) 0002-7863 (Linking). doi: 10.1021/jacs.2c02096. URL https://www.ncbi.nlm.nih.gov/pubmed/35713375.

[119] Emily R. Draper and Dave J. Adams. Low-molecular-weight gels: The state of the art. *Chem*, 3(3):390–410, 2017. ISSN 24519294. doi: 10.1016/j.chempr.2017.07.012.

[120] Wenhan Li, Quanchi Chen, Yanyu Ma, Haiwen Su, Haoyu Ren, and Huan Wang. Antibacterial hydrogels for bacteria-infected wound treatment. *Biomedical Technology*, 9, 2025. ISSN 2949723X. doi: 10.1016/j.bmt.2024.11.001.

[121] Ping Zhang, Wenjie Xiong, Mingzhen Shi, Zhuoheng Tu, Xingbang Hu, Xiaomin Zhang, and Youting Wu. Natural deep eutectic solvent-based gels with multi-site interaction mechanism for selective membrane separation

of so2 from n2 and co2. *Chemical Engineering Journal*, 438, 2022. ISSN 13858947. doi: 10.1016/j.cej.2022.135626.

[122] A. Y. Tam and V. W. Yam. Recent advances in metallogels. *Chem Soc Rev*, 42(4):1540–67, 2013. ISSN 1460-4744 (Electronic) 0306-0012 (Linking). doi: 10.1039/c2cs35354g. URL `https://www.ncbi.nlm.nih.gov/pubmed/23296361`.

[123] Bjorn Joos, Thomas Vranken, Wouter Marchal, Mohammadhosein Safari, Marlies K. Van Bael, and An T. Hardy. Eutectogels: A new class of solid composite electrolytes for li/li-ion batteries. *Chemistry of Materials*, 30(3): 655–662, 2018. ISSN 0897-4756 1520-5002. doi: 10.1021/acs.chemmater.7b03736.

[124] Carmen C. Piras, Paul G. Genever, and David K. Smith. Combining gellan gum with a functional low-molecular-weight gelator to assemble stiff shaped hybrid hydrogels for stem cell growth. *Materials Advances*, 3 (21):7966–7975, 2022. ISSN 2633-5409. doi: 10.1039/d2ma00565d.

[125] Hina Goyal, Sanya Pachisia, and Rajeev Gupta. Systematic design of a low-molecular-weight gelator and its application in the sensing and retention of residual antibiotics. *Crystal Growth & Design*, 20(9):6117–6128, 2020. ISSN 1528-7483 1528-7505. doi: 10.1021/acs.cgd.0c00820.

[126] Y. Shi, Z. Wang, X. Zhang, T. Xu, S. Ji, D. Ding, Z. Yang, and L. Wang. Multi-responsive supramolecular hydrogels for drug delivery. *Chem Commun (Camb)*, 51(83):15265–7, 2015. ISSN 1364-548X (Electronic) 1359-7345 (Linking). doi: 10.1039/c5cc05792b. URL `https://www.ncbi.nlm.nih.gov/pubmed/26329300`.

[127] H. Mehdi, H. Pang, W. Gong, M. K. Dhinakaran, A. Wajahat, X. Kuang, and G. Ning. A novel smart supramolecular organic gelator exhibiting dual-channel responsive sensing behaviours towards fluoride ion via gel-gel states. *Org Biomol Chem*, 14(25):5956–64, 2016. ISSN 1477-0539 (Electronic) 1477-0520 (Linking). doi: 10.1039/c6ob00600k. URL `https://www.ncbi.nlm.nih.gov/pubmed/27193611`.

[128] P. Sutar and T. K. Maji. Coordination polymer gels: soft metal-organic supramolecular materials and versatile applications. *Chem Commun (Camb)*, 52(52):8055–74, 2016. ISSN 1364-548X (Electronic) 1359-7345 (Linking). doi: 10.1039/c6cc01955b. URL `https://www.ncbi.nlm.nih.gov/pubmed/27203359`.

[129] George P. T. Roddy, Livia Salvati Manni, Rob Atkin, and Gregory G. Warr. 12-hydroxyoctadecanoic acid forms two kinds of supramolecular gels in nanostructured protic ionic liquids. *Journal of Colloid and Interface Science*, 691, 2025. ISSN 00219797. doi: 10.1016/j.jcis.2025.137384.

[130] M. Burkhardt, S. Kinzel, and M. Gradzielski. Macroscopic properties and microstructure of hsa based organogels: sensitivity to polar additives. *J Colloid Interface Sci*, 331(2):514–21, 2009. ISSN 1095-7103 (Electronic) 0021-9797 (Linking). doi: 10.1016/j.jcis.2008.11.078. URL `https://www.ncbi.nlm.nih.gov/pubmed/19144353`.

[131] Malvern Instruments. *Rheology Primer*. Malvern. Malvern Panalytical, Malvern, Worcestershire, 2016. URL `www.malvern.com`.

[132] Fridjtov Irgens. *Rheology and Non-Newtonian Fluids*. Springer, 2014. ISBN 978-3-319-01052-6. doi: 10.1007/978-3-319-01053-3.

[133] Mónia A. R. Martins, Simão P. Pinho, and João A. P. Coutinho. Insights into the nature of eutectic and deep eutectic mixtures. *Journal of Solution Chemistry*, 48(7):962–982, 2018. ISSN 0095-9782 1572-8927. doi: 10.1007/s10953-018-0793-1.

[134] Dannie J. G. P. van Osch, Lawien F. Zubeir, Adriaan van den Bruinhorst, Marisa A. A. Rocha, and Maaike C. Kroon. Hydrophobic deep eutectic solvents as water-immiscible extractants. *Green Chemistry*, 17(9):4518–4521, 2015. ISSN 1463-9262 1463-9270. doi: 10.1039/c5gc01451d.

[135] J. C. Lutter, T. Y. Wu, and Y. Zhang. Hydration of cations: a key to understanding of specific cation effects on aggregation behaviors of peo-ppo-peo triblock copolymers. *J Phys Chem B*, 117(35):10132–41, 2013. doi: 10.1021/jp405709x. URL `https://www.ncbi.nlm.nih.gov/pubmed/23931074`.

[136] H. I. Okur, J. Hladilkova, K. B. Rembert, Y. Cho, J. Heyda, J. Dzubiella, P. S. Cremer, and P. Jungwirth. Beyond the hofmeister series: Ion-specific effects on proteins and their biological functions. *J Phys Chem B*, 121(9):1997–2014, 2017. doi: 10.1021/acs.jpcb.6b10797. URL `https://www.ncbi.nlm.nih.gov/pubmed/28094985`.

[137] J. C. Araque, J. J. Hettige, and C. J. Margulis. Modern room temperature ionic liquids, a simple guide to understanding their structure and how it may relate to dynamics. *J Phys Chem B*, 119(40):12727–40, 2015. doi: 10.1021/acs.jpcb.5b05506. URL `https://www.ncbi.nlm.nih.gov/pubmed/26244375`.

[138] M. Almeida, D. Dudzinski, C. Amiel, J. M. Guigner, S. Prevost, C. Le Coeur, and F. Cousin. Aqueous binary mixtures of stearic acid and its hydroxylated counterpart 12-hydroxystearic acid: Cascade of morphological transitions at room temperature. *Molecules*, 28(11), 2023. doi: 10.3390/molecules28114336. URL `https://www.ncbi.nlm.nih.gov/pubmed/37298812`.

[139] Anne-Laure Fameau and Michael A. Rogers. The curious case of 12-hydroxystearic acid — the dr. jekyll & mr. hyde of molecular gelators. *Current Opinion in Colloid & Interface Science*, 45:68–82, 2020. ISSN 13590294. doi: 10.1016/j.cocis.2019.12.006.

[140] Thomas Gerlach, Simon Müller, Andrés González de Castilla, and Irina Smirnova. An open source cosmo-rs implementation and parameterization supporting the efficient implementation of multiple segment descriptors. *Fluid Phase Equilibria*, 560, 2022. ISSN 03783812. doi: 10.1016/j.fluid.2022.113472.

[141] Frank Neese. The orca program system. *WIREs Computational Molecular Science*, 2(1):73–78, 2011. ISSN 1759-0876 1759-0884. doi: 10.1002/wcms.81.